

INFORMATION TO USERS

This manuscript has been reproduced from the microfilm master. UMI films the text directly from the original or copy submitted. Thus, some thesis and dissertation copies are in typewriter face, while others may be from any type of computer printer.

The quality of this reproduction is dependent upon the quality of the copy submitted. Broken or indistinct print, colored or poor quality illustrations and photographs, print bleedthrough, substandard margins, and improper alignment can adversely affect reproduction.

In the unlikely event that the author did not send UMI a complete manuscript and there are missing pages, these will be noted. Also, if unauthorized copyright material had to be removed, a note will indicate the deletion.

Oversize materials (e.g., maps, drawings, charts) are reproduced by sectioning the original, beginning at the upper left-hand corner and continuing from left to right in equal sections with small overlaps. Each original is also photographed in one exposure and is included in reduced form at the back of the book.

Photographs included in the original manuscript have been reproduced xerographically in this copy. Higher quality 6" x 9" black and white photographic prints are available for any photographs or illustrations appearing in this copy for an additional charge. Contact UMI directly to order.

UMI

A Bell & Howell Information Company
300 North Zeeb Road, Ann Arbor MI 48106-1346 USA
313/761-4700 800/521-0600

UNIVERSITY OF ALBERTA

A STUDY OF THE MECHANICAL BEHAVIOUR OF NETWORKS

BY

XINAN ZHOU ©

A thesis submitted to the Faculty of Graduate Studies and Research in partial fulfillment of the requirements for the degree of Master of Science.

DEPARTMENT OF MECHANICAL ENGINEERING

Edmonton, Alberta

Spring, 1998



National Library
of Canada

Acquisitions and
Bibliographic Services

395 Wellington Street
Ottawa ON K1A 0N4
Canada

Bibliothèque nationale
du Canada

Acquisitions et
services bibliographiques

395, rue Wellington
Ottawa ON K1A 0N4
Canada

Your file Votre référence

Our file Notre référence

The author has granted a non-exclusive licence allowing the National Library of Canada to reproduce, loan, distribute or sell copies of this thesis in microform, paper or electronic formats.

The author retains ownership of the copyright in this thesis. Neither the thesis nor substantial extracts from it may be printed or otherwise reproduced without the author's permission.

L'auteur a accordé une licence non exclusive permettant à la Bibliothèque nationale du Canada de reproduire, prêter, distribuer ou vendre des copies de cette thèse sous la forme de microfiche/film, de reproduction sur papier ou sur format électronique.

L'auteur conserve la propriété du droit d'auteur qui protège cette thèse. Ni la thèse ni des extraits substantiels de celle-ci ne doivent être imprimés ou autrement reproduits sans son autorisation.

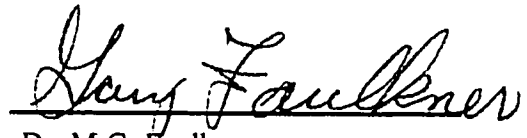
0-612-29003-4

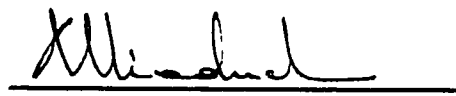
Canada


UNIVERSITY OF ALBERTA

FACULTY OF GRADUATE STUDIES AND RESEARCH

The undersigned certify that they have read, and recommend to the Faculty of Graduate Studies and Research for acceptance, a thesis entitled A STUDY OF THE MECHANICAL BEHAVIOUR OF NETWORKS submitted by XINAN ZHOU in partial fulfillment of the requirements for the degree of Master of Science.


Dr. M.G. Faulkner


Dr. A. Mioduchowski


Dr. C.-Q. Ru


Dr. R.J. Tait

Date Jan. 15, 1998

This is dedicated to all my teachers.

ABSTRACT

In this work, the continuous model is used to study the mechanical behaviours of networks. In the cases of plane reference configurations, the deformations of networks under prescribed displacements, static loads and punching loads are studied. The effects of elasticity, elastic-plasticity, and visco-elastic-plasticity are described by the mechanical sublayer model. For the low velocity punching case, a simple way to approximate the process is put forward. Explicit Lagrangian Finite Difference Methods, which are in conservative form, are used in the plane reference configuration cases. These methods are further used in the cases of the circular cylinder reference configuration. Dynamic Relaxation Methods are used to solved the non-linear algebraic equations, which are obtained after space domain discretization. Some interesting numerical examples are provided. Also some experiences of choosing fictitious density and fictitious mass are presented.

Acknowledgment

I would like to express my deepest gratitude to Dr. D.J. Steigmann, who supervised this thesis, for his guidance and support.

I also wish to thank Dr. P. Schiavone, for his advice and encouragement throughout my program at the University of Alberta, and all the professors in the Department of Mechanical Engineering who gave me advice in the course of my research.

With pleasure I do acknowledge the services of Saulo Oduor and Mohiuddin Mala, both for proof-reading the thesis, and Qianhong Zhuang for her help in latex.

Table of Contents

Chapter 1	Backgrounds	1
Chapter 2	Numerical Methods	4
2.1	Explicit Lagrangian Finite Difference Methods	4
2.2	Dynamic Relaxation Method	6
2.3	Mechanical Sublayer Model	11
Chapter 3	Equations for Arbitrary Networks	14
Chapter 4	Plane Reference Configuration	18
Chapter 5	Circular Cylinder Reference Configuration	27
Chapter 6	Conclusions and Remarks	30
Reference		55

List of Figures

Figure 1:	A grid cell of ELFD	5
Figure 2a:	Unit square reference plane	10
Figure 2b:	Stretching shape of unit square network	10
Figure 2c:	Stretching shape of unit square network	10
Figure 3a:	s-s curves of 3 sublayers	12
Figure 3b:	s-s curve modeled by 3 sublayers	12
Figure 4a:	Strain rate dependent s-s curves of k-th layer	13
Figure 4b:	Strain rate dependent s-s curves modeled by 3 sublayers	13
Figure 5:	Finite difference mesh	21
Figure 6:	Shape with point load at center	32
Figure 7:	Shape with point load at center and pressure	32
Figure 8:	Shape with point load at center and pressure	33
Figure 9:	Deformed shape of circular network	33
Figure 10:	Mesh for triangular domain	34
Figure 11:	Deformed shape of triangle network	34
Figure 12:	Mesh for ellipse domain	35
Figure 13:	Deformed shape of ellipse network	35
Figure 14:	Deformed shape of ellipse network	36
Figure 15a:	Mesh one for L-domain	36
Figure 15b:	Mesh two for L-domain	37
Figure 15c:	Mesh three for L-domain	37
Figure 16a:	Deformed shape with mesh 1	38
Figure 16c:	Deformed shape with mesh 2	38
Figure 16c:	Deformed shape with mesh 3	39
Figure 17:	Deformed shape of 4-family fiber network	39

Figure 17a:	Defromed shape after being stretched	40
Figure 18:	Deformed shape of 4-family fiber network	40
Figure 19:	Deformed shape of unit square network	41
Figure 20:	Deformed shape of unit square network	41
Figure 21:	Deformed shape in plastic range	42
Figure 22:	Residual shape after unloading	43
Figure 23:	Load-displacement relationship	43
Figure 24:	Deformed shape of unit circle network	44
Figure 25:	Residual shape of unit circle network	44
Figure 26:	Load-displacement relationship	45
Figure 27:	Deformed shape of unit square network	45
Figure 28:	Deformed shape of unit square network after unloading	46
Figure 29:	Deformed shape independent of strain rate	46
Figure 30:	Deformed shape dependent of strain rate	47
Figure 31:	Deformed shape when $h\nu=0.1$	47
Figure 32:	Deformed shape when $h\nu=0.01$	48
Figure 33:	Deformed shape when $h\nu=0.001$	48
Figure 34:	Deformed shape at initial punching stage	49
Figure 35:	Deformed shape at broken stage	49
Figure 36:	Static load-displacement relationship	50
Figure 37:	Motion of the mass	50
Figure 38:	Deformed shape after being impacted	51
Figure 39:	Deformed shape of unit square network	51
Figure 40:	Deformed shape of unit square network	52
Figure 41:	Deformed shape of circular cylinder network	52
Figure 42:	Deformed shape of circular cylinder network	53
Figure 43:	Deformed shape of circular cylinder network	53
Figure 44:	Deformed shape of circular cylinder network	54
Figure 45:	Deformed shape of circular cylinder network	54

Chapter 1. Background

The term “network” denotes a system of flexible fibers directed along two or more one-parameter families of lines on a surface. The networks usually have regular patterns repeating themselves symmetrically. These patterns are required partly by practical manufacturing processes, partly by aesthetic considerations and partly by the need to stiffen the assembly and strengthen it to withstand loads.

The networks are kinds of membrane structures which are often called suspension or pneumatic structures. Membrane structures have long been used, as is shown in their employment for nomads’ tents, military camps, sails, filters, etc.. In modern civil engineering they are used for spanning large spaces, such as sports facilities and exhibition pavilions. Their clear advantages are their light weight, applicability to form a variety of shapes and sizes, and suitability for prefabrication. We also find membrane structures in the biomedical field. Researchers have studied the problems of human fetal membranes, the balloon pumps as heart-assist devices, the strength of red-cell membranes, the mechanical behaviour of alveolar cells in the lung, etc..

There are two parallel methods in the study of networks. One is the discrete method, which treats fibers as a disconnected assembly and studies the details of each single fiber, as in the work of Hearle [1969,1980]. The discrete method is mostly used in fabric engineering, which designs and produces textiles, and is sometimes used in the analysis of cable-nets. More information about the discrete method can be found in Hearle [1969, 1980]. The other method is the continuous one, which regards fibers as continuously distributed and forming a continuous surface. Thus, the use of continuous theory is practical.

There are two distinct approaches in the study of membrane structures. One approach treats the membrane as a specific case of a shell of zero thickness by suppressing the bending moments and transverse shears. It is then called a shell membrane. Another approach regards networks or membranes as two-dimensional deformable sheets, which are plane or curved, and incapable of carrying any stress couples or transverse shears. These sheets can sustain only

a tangential resultant force and are usually called "ideal" or "pure" membranes.

Ideal membranes are different from shell membranes in several respects. 1. Ideal membranes cannot sustain compressive stresses, whereas shell membranes can carry compressive stresses until buckling takes place; 2. large inextensional deformations can be sustained in an ideal membrane, but not in a shell membrane, etc.. It is difficult to say which one is more exact, as no references are available to compare the two models.

The main characteristic of membrane structures is the large deformation, i.e. geometrical nonlinearities sometimes accompanied by material nonlinearities. To capture the geometric nonlinearity for shell membranes, we seek help from Von Karman's large deflection flat plate equations or Berger's equations for the large deflection of a thin elastic isotropic plate of uniform thickness by making the bending stiffness zero as in the work of Jones [1974]. A well-known nonlinear membrane theory was developed by Föppl [1907]. Results were obtained by Paul [1977] using this theory. The theory results from the Von Karman's nonlinear plate theory. According to this theory, linear stress strain relations are assumed, and tangential displacements are assumed to be small compared with the normal displacement (i.e. small strains) in addition to the usual thin shell approximations. Later, Berger [1955] introduced the assumption that the first invariant of the strain tensor is constant in order to get solutions for some specific cases. But it is still difficult to obtain analytical solutions for many cases. With the advent of high speed computers, the Finite Element Method(FEM) was found to be an appropriate tool for design analyses of membrane structures. Nonlinear analysis programs, first devised to find the shapes of shells, were adapted to treat both shape finding and load analysis of membrane structures. Several finite element solutions for the deformation analysis of elastic membranes were presented by Oden [1972]. Han and Olson [1987] also provided a finite element solution for wind loaded pneumatic membrane structures. Numerous studies of shell membranes have been published. Only a simple outline has been given above.

The first ideal membrane model, also known as the Tchebychev net, was suggested by Tchebychev [1878]. It was used to study cloth which deformed

mainly as a result of changes in the angle between the threads of the warp and woof. The additional deformation due to fiber stretching is ordinarily negligible in comparison to the finite distortion that can be produced without stretching. This model treats fibers as being inextensible and distributed continuously. Rivlin [1955] used the same continuum model in studying the problem of plain strain and got a general solution. Adkins [1956a,1956b] generalized this theory. Genensky and Rivlin [1959] extended this model to elastic networks of infinitesimal plane strain. Green and Shi [1990] considered the effects of elasticity in the context of a general theory for plane deformations. Steigmann and Pipkin [1991] developed this theory further and extended it to account for arbitrary deformations of curved surfaces. From the latter theory, Steigmann [1992] developed a linear theory for small displacements superposed on finite deformations of elastic networks. The above studies of pure membranes are all analytical. Many problems, however, cannot be solved in this way. Based on Steigmann's work [1992], Meiping [1993] did modal analysis of a prestressed hyperbolic paraboloid network. Haseganu and Steigmann [1994] were the first to introduce the conserved form of finite difference and DR into the numerical study of pure membranes, a method which proved to be easy and effective. Haseganu and Steigmann [1996] also studied the finitely deformed elastic networks using the same method.

The same numerical method as developed by Haseganu and Steigmann [1994] is used in this work to study the plastic case, the low speed punching case, the concentrated load case, and the circular cylinder reference configuration case.

Chapter 2. Numerical Methods

2.1 Explicit Lagrangian Finite Difference Methods

The equilibrium equations of networks are nonlinear for large deformations. These equations do not usually have any analytical solutions and therefore must be solved by numerical methods. The Finite Element Method(FEM) is widely used because of its advantages: 1. it is easy to discretize the domain with different types of elements or a combination of several types of elements to fit the shape of the arbitrary domain; 2. it is easy to adjust the element type to meet different load cases; 3. many popular commercial FE codes, such as ANSYS and SAP, have the function of analysing membrane structures. They all are based on shell membrane theory and thus have restrictions when used for the deformation of the membranes.

Another popular numerical method is the Finite Difference Method(FDM), which directly replaces the original differential equations with finite difference forms and which is easy to carry out. Few cases can be found regarding its applications in calculating membrane structures. General finite difference grids are rectangular in order to express derivatives at a point with adjacent grid points. So if the domain is not a regular shape, generation of the mesh grids becomes very difficult. But the Explicit Lagrangian Finite Difference Methods [Herrmann and Bertholf 1983] are of conservative form, combining the advantages of FEM and FDM. The basic idea is to use Green's theorem to express the derivatives at the center of the cell with the grid points. The cell does not need to be rectangular; it can even be triangular or polygonal. Fig.1 shows a grid cell.

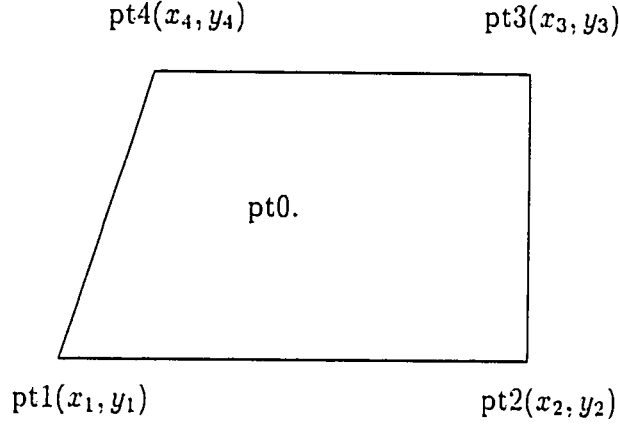


Fig.1 A grid cell for integral

The coordinates of points 1, 2, 3, and 4 are (x_1, y_1) , (x_2, y_2) , (x_3, y_3) , (x_4, y_4) respectively. The values of function ϕ at points with these coordinates are ϕ_1 , ϕ_2 , ϕ_3 , ϕ_4 respectively. Then

$$\begin{aligned}
 \iint \frac{\partial \phi}{\partial x} dx dy &= \oint \phi dy \\
 &= \frac{(\phi_1 + \phi_2)}{2}(y_2 - y_1) + \frac{(\phi_3 + \phi_2)}{2}(y_3 - y_2) \\
 &\quad + \frac{(\phi_3 + \phi_4)}{2}(y_4 - y_3) + \frac{(\phi_1 + \phi_4)}{2}(y_1 - y_4) \\
 &= \frac{1}{2}[(y_2 - y_4)(\phi_1 - \phi_3) - (y_1 - y_3)(\phi_2 - \phi_4)].
 \end{aligned} \tag{2.1}$$

By average principle,

$$\iint \left(\frac{\partial \phi}{\partial x}\right) dx dy = A \left(\frac{\partial \phi}{\partial x}\right)_0.$$

, where A is the area of the grid cell. Using Green's theorem, we can express A as

$$\begin{aligned}
 A &= \iint dx dy \\
 &= \frac{1}{2} \oint x dy - y dx \\
 &= \frac{1}{2}[(y_2 - y_4)(x_1 - x_3) - (y_1 - y_3)(x_2 - x_4)],
 \end{aligned} \tag{2.2}$$

so that

$$\left(\frac{\partial \phi}{\partial x}\right)_0 = \frac{1}{2A}[(y_2 - y_4)(\phi_1 - \phi_3) - (y_1 - y_3)(\phi_2 - \phi_4)]. \tag{2.3}$$

Similarly, we have

$$\left(\frac{\partial \phi}{\partial y}\right)_0 = \frac{1}{2A}[(\phi_2 - \phi_4)(x_1 - x_3) - (\phi_1 - \phi_3)(x_2 - x_4)]. \quad (2.4)$$

A different method of deduction and more details can be found in Herrmann and Bertholf [1983].

2.2 Dynamic Relaxation Method

With the help of the finite difference schemes above, the nonlinear differential equilibrium equations can be changed into a set of simultaneous algebraic nonlinear equations such as

$$\mathbf{F}(\mathbf{x}) = \mathbf{0}. \quad (2.5)$$

In the finite element method, the Newton Raphson method is often used to solve the set of nonlinear algebraic equations. It is very tedious to calculate the Jacobi matrix, which is called the “tangential stiffness matrix” in structural mechanics. It also requires a lot of computer memory to store the matrix. Dynamic Relaxation (DR) can overcome these shortcomings. The basic idea behind DR is to add inertia and friction terms to the static equation to get a dynamic equation. The solution of the static equation is the steady solution of the dynamic equation. So $\mathbf{F}(\mathbf{x}) = \mathbf{0}$ becomes

$$\mathbf{M}\ddot{\mathbf{x}} + \mathbf{C}\dot{\mathbf{x}} + \mathbf{F}(\mathbf{x}) = \mathbf{0}, \quad (2.6)$$

where \mathbf{M} is a diagonal mass matrix, $\mathbf{C} = c\mathbf{M}$, where c is a constant friction coefficient. The superimposed dot indicates the derivative of \mathbf{x} with respect to time t . The expressions of the central difference for a time step h and at n th time increment are:

$$\dot{\mathbf{x}}^n = \frac{1}{2}(\dot{\mathbf{x}}^{n+0.5} + \dot{\mathbf{x}}^{n-0.5}), \quad (2.7)$$

$$\ddot{\mathbf{x}}^n = h^{-1}(\dot{\mathbf{x}}^{n+0.5} - \dot{\mathbf{x}}^{n-0.5}), \quad (2.8)$$

$$\dot{\mathbf{x}}^n = h^{-1}(\mathbf{x}^{n+0.5} - \mathbf{x}^{n-0.5}). \quad (2.9)$$

Substitution into the dynamic equations above yields the fully explicit algorithm

$$\dot{\mathbf{x}}^{n+0.5} = \frac{2 - ch}{2 + ch} \dot{\mathbf{x}}^{n-0.5} - \frac{2h}{2 + ch} \mathbf{M}^{-1} \mathbf{F}(\mathbf{x}^n). \quad (2.10)$$

$$\mathbf{x}^{n+1} = \mathbf{x}^n + h \dot{\mathbf{x}}^{n+0.5}. \quad (2.11)$$

The mass \mathbf{M} and friction coefficient c need not be the true ones for static problems. By trial and error, we can obtain the appropriate \mathbf{M} and c to make the iteration converge more quickly. More details can be found in Underwood [1983].

We now discuss how to eliminate the pseudo plastic accumulation in the DR method. When the network is only within the elastic range, the loading and unloading paths of the fibers are the same. The stress strain(s-s) relationship is a single value function, so that the transient solution of DR always decays to the right static solution. Furthermore, it is independent of the loading order and initial velocities. But when the network is beyond the elastic range, i.e., in the plastic range, then the loading and unloading paths are not the same, and the stress and strain(s-s) function becomes multi valued. In the decay process of a transient solution of DR to a static solution, artificial plastic accumulation will occur, and thus DR will give an incorrect static result. In the early stages of DR applications, the constitutive equations are linear elastic. Rushton and Hook [1974] were probably the first to use DR in geometrically nonlinear problems with simultaneous nonlinear stress-strain relationships. In their work, the total deformation formulae are used, with the s-s law given as $\sigma = B\epsilon^n$ and simple loading is assumed. The problems can then be treated as nonlinear elastic ones. DR schemes are similar to those of geometrically nonlinear and physically linear problems. The problem of combining geometric nonlinearity and elasto-plastic material properties with complex loading was first analysed with DR by Harding et al. [1977]. Later many works on this topic were published. Basically, there are two ways to implement DR:

- (a) Total Deformation Method
- (b) Incremental Method

The total deformation method is easy to implement but has two apparent shortcomings: (1) it is incapable of taking proper account of any local elastic unloading in the plastic range; (2) even if monotonic proportional static loading is applied, the final settled state determined by DR may differ from the true state. The second limitation is caused by the false plastic accumulation of DR, but can be corrected by treating the elasto-plastic s-s relationship as a nonlinear elastic s-s law, i.e., loading and unloading are in the same path. But the first shortcoming is a fatal one. It cannot be avoided for complex loading cases.

The incremental method can overcome the shortcomings of the total deformation method, so it is a popular method for tracing the whole loading process. Generally there are two ways to implement (b):

1. all governing equations are in incremental forms [Harding and Hobbs 1977; Lim and Turvey 1984]; and
2. constitutive equations are in incremental forms, equilibrium equations are in total displacement forms, and the strain increments are expressed by the displacements before the load step and the displacements after the load step [Frieze, et al. 1978; key, et al. 1981; Cardis and Frieze 1988].

In our case, the incremental equilibrium equations of networks are too complicated to be carried out numerically, so we used the second method. In seeking the equilibrium position, the function of DR is the same as Newton-Raphson method. During iteration of the n th load step, the tangential stiffness at the start of this load step remains constant, until the velocities are smaller than the tolerance. If the material is linear elastic, then each load step, the converged point obtained by using DR once is on the right path. If the material is in the plastic range, the point will deviate from the true path. The tangential stiffness at the converged point has to be updated and DR is used again to approach the right position within the same load level until the change of displacements is within the tolerance. This is called “double loops” in each load level [Bushell 1977]. Many papers on DR do not mention

this “double loops” method, and use only a single loop, so they are only linear approximations. After DR converges, we calculate the new displacements, strains and stresses. In most work, the DR method has been applied with the one step method, i.e., assuming the strain increment perpendicular to the yielding surface for each load step. Only Key. et al. [1981] introduced the sub-increment concept from Bushell [1977] for higher accuracy requirements. This is a significant development: firstly, constitutive evaluation is disassociated from the load incrementation and related equilibrium iteration procedure; secondly, the strain increment is subdivided into sub-increments, each sub-increment is perpendicular to the yielding surface, so that the path of total strain increment need not be a straight line segment. One important point that should be kept in mind when the incremental method is used is that we need to be clear about which point is loading and which one is unloading in the plastic range. In the plastic range, the different modulus is used in constitutive equations for loading and unloading paths, and the yielding stresses need to be updated for the unloading points.

Adaptation in this work

For our case, though the problems are 3-D, the constitutive equation of each fiber is 1-D, and we do not need to assemble a stiffness matrix for DR, so we associate the constitutive equation with the DR in each load step. Loading and unloading are judged with reference to the state at the end of the last load step. The loading path follows the real stress-strain curve, while unloading path follows the elastic straight line. When DR converges, we get the new stresses, strains and displacements at the same time, making this method efficient. We also implemented the method which disassociates the constitutive equation from the DR iteration, but doing so takes longer. If the fibers are elastic perfectly plastic materials and we fix one end of the networks and stretch uniformly at the other end so that the fibers are in the plastic range, then we find that the method does not give a uniform strain field. If we always use the elastic modulus at each load step, though it takes four times longer, a uniform strain field is obtained. It may be said that a uniform plastic strain

field is not practical. But here the intention is to display the special numerical phenomena. The reference configuration is a plane unit square network of two families of fibers; one family is parallel to the x-axis, and the other is parallel to the y-axis. Sides AB and CD are fixed, while sides DA and BC are free. Side AB moves out a distance. Fig.2b shows the shape realised by the first method using the tangential modulus; Fig.2c shows the shape realised by the second method using the elastic modulus.

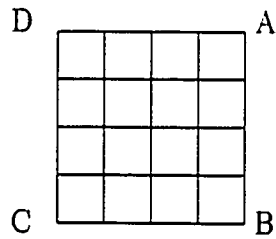


Fig.2a Reference Configuration

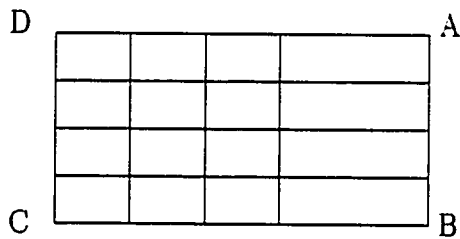


Fig.2b

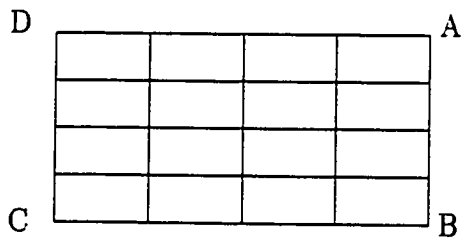


Fig.2c

2.3 Mechanical Sublayer Model

There are several ways to describe the stress-strain relationship in numerical calculations, but the mechanical sublayer model is more convenient. It can easily include the plastic and visco-elastic-plastic effects. In this work only a one-dimensional constitutive equation is used, so we give only a simple explanation of the sublayer model in one-dimension. More information about the 3-D sublayer model can be found in Gupta, et al. [1980].

In the mechanical sublayer model, the uniaxial tension test stress-strain curve of the material is first approximated by $n + 1$ piece-wise-linear segments which are defined at coordinates (σ_k, ϵ_k) , $k = 1, 2, \dots, n$. Then the material is envisioned as consisting, at any point in the material, of n equally-strained "sublayers" of elastic perfectly plastic material, with each sublayer having the same elastic modulus E , but a different yield stress. For the k th sublayer, the yield stress $\sigma_{yk} = E\epsilon_k$, $k = 1, 2, \dots, n$. The stress value σ_k^s of the k th sublayer can be defined uniquely by the strain history and the value of strain and the strain rate present at that point. The stress, σ , at that point corresponding to strain ϵ may be expressed as

$$\sigma = \sum_{k=1}^n c_k \sigma_k^s(\epsilon), \quad (2.12)$$

where c_k , the weighting factor for each sublayer, is given by

$$c_k = \frac{E_k - E_{k+1}}{E}, \quad (2.13)$$

where

$$\begin{aligned} E_1 &= E, \\ E_k &= \frac{\sigma_k^s - \sigma_{k-1}^s}{\epsilon_k - \epsilon_{k-1}}, \\ k &= 2, 3, \dots, n, \\ E_{n+1} &= 0. \end{aligned}$$

For example, when $n=3$, Fig.3a shows the three perfectly plastic sublayers at different yielding points and Fig.3b shows the s-s curve modeled by the three sublayers.

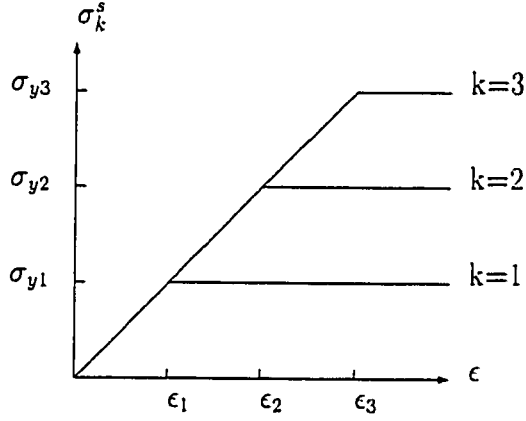


Fig.3a s-s curves of sublayers

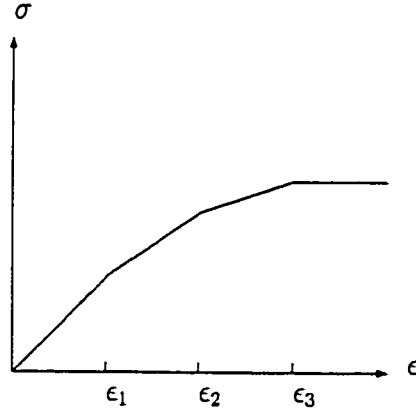


Fig.3b s-s curve modeled by 3 sublayers

From a computational point of view, the mechanical sublayer model is convenient for problems with general loading paths such as loading, unloading, reloading, and cyclic loading. It follows the kinematic hardening rule, so it can express the Baushinger effect. It can also easily accommodate the strain rate effect. Fig.4b illustrates the one-dimensional s-s curves of strain rate dependence. For the k th sublayer, it is elastic perfectly plastic, and its yield point changes with the strain rate $\dot{\epsilon}$, according to

$$\sigma_y = \sigma_0 \left(1 + \left| \frac{\dot{\epsilon}}{D} \right|^{\frac{1}{p}} \right). \quad (2.14)$$

Each sublayer has the same constants D and p , which are obtained experimentally. For simplicity, we set $D = p = 1$, and two strain rates, r_1 , r_2 , and $0 < r_1 < r_2$, as shown in Fig.4a and Fig.4b.

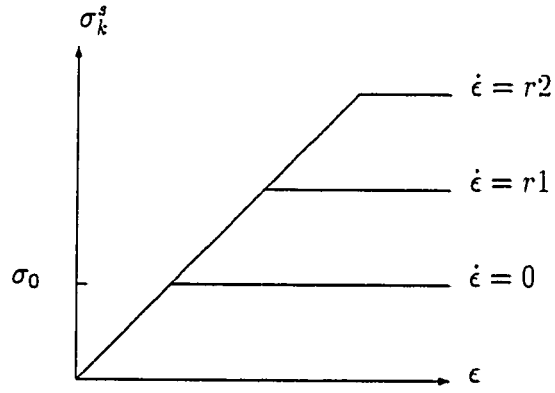


Fig.4a strain rate dependent s-s curves of k th layer

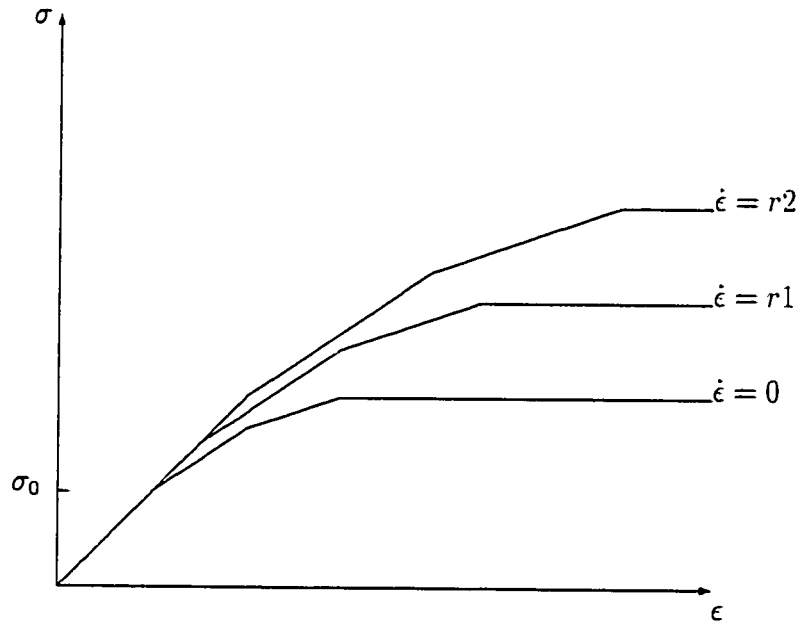


Fig.4b strain rate dependent s-s curve modeled by 3 sublayers

This sublayer model is included in the computing code.

Chapter 3. Equations for Arbitrary Networks

Before we discuss the networks of plane reference configuration and circular cylinder reference configuration, it is necessary to state the equations for arbitrary networks, from which the equations for any specific case can be deduced. Details can be found in Steigmann and Pipkin [1991].

Gauss coordinates θ^α ($\alpha = 1, 2$) on the membrane surface are used. Given a material point p with coordinates θ^α from its reference position $\mathbf{x}(\theta^1, \theta^2)$ to the place $\mathbf{r}(\theta^1, \theta^2)$, the natural basis \mathbf{a}_α is defined by

$$\mathbf{a}_\alpha = \mathbf{r}_{,\alpha}, \quad (3.1)$$

which spans the tangent plane of the deformed surface at p . Commas are used to denote partial derivatives with respect to θ^α . Then

$$d\mathbf{r} = \mathbf{a}_\alpha d\theta^\alpha \quad (3.2)$$

and

$$|d\mathbf{r}|^2 = a_{\alpha\beta} d\theta^\alpha d\theta^\beta, \quad (3.3)$$

where

$$a_{\alpha\beta} = \mathbf{a}_\alpha \cdot \mathbf{a}_\beta, \quad (3.4)$$

is the metric tensor, and $a = \det(a_{\alpha\beta})$. When $a > 0$, the reciprocal metric components $a^{\alpha\beta}$ are uniquely defined by the relation

$$a^{\alpha\gamma} a_{\gamma\alpha} = \delta_\beta^\alpha, \quad (3.5)$$

where δ_β^α is the Kronecker delta. The reciprocal basis \mathbf{a}^α is given by

$$\mathbf{a}^\alpha = a^{\alpha\beta} \mathbf{a}_\beta. \quad (3.6)$$

The normal unit $\mathbf{n}(\theta^1, \theta^2)$ on the deformed surface is given by

$$\mathbf{n} = \frac{1}{2} \epsilon^{\alpha\beta} \mathbf{a}_\alpha \times \mathbf{a}_\beta, \quad (3.7)$$

where $\epsilon_{\alpha\beta} = a^{\frac{1}{2}} e_{\alpha\beta}$, $\epsilon^{\alpha\beta} = a^{-\frac{1}{2}} e^{\alpha\beta}$, and $e^{\alpha\beta} = e_{\alpha\beta}$ is the unit alternator.

Corresponding results for the reference surface are

$$\left\{ \begin{array}{ll} \mathbf{A}_\alpha = \mathbf{X}_{, \alpha}, & A_{\alpha\beta} = \mathbf{A}_\alpha \cdot \mathbf{A}_\beta, \\ A = \det(A_{\alpha\beta}), & A^{\alpha\gamma} A_{\gamma\beta} = \delta_\beta^\alpha, \\ \mathbf{A}_\alpha = A^{\alpha\beta} \mathbf{A}_\beta, & \mu_{\alpha\beta} = A^{\frac{1}{2}} e_{\alpha\beta}, \\ \mu^{\alpha\beta} = A^{-\frac{1}{2}} e^{\alpha\beta}, & \mu_{\alpha\beta} \mathbf{N} = \mathbf{A}_\alpha \times \mathbf{A}_\beta. \end{array} \right\} \quad (3.8)$$

We regard the network as a 2-D elastic continuum with a strain energy W , measured per unit area of reference surface. The deformation gradient, \mathbf{F} , is defined by

$$d\mathbf{r} = \mathbf{F} d\mathbf{x}, \quad (3.9)$$

and

$$\mathbf{F} = \mathbf{a}_\alpha \otimes \mathbf{A}^\alpha; \quad \mathbf{a}_\alpha = \mathbf{F} \mathbf{A}_\alpha. \quad (3.10)$$

The Piola stress \mathbf{T} is defined by

$$\mathbf{T} = \mathbf{T}^\alpha \otimes \mathbf{A}_\alpha; \quad \mathbf{T}^\alpha = (\partial W / \partial r^i_{, \alpha}) \mathbf{e}_i. \quad (3.11)$$

We assume that W is frame-indifferent, i.e. $W(\mathbf{F}) = W(\mathbf{Q}\mathbf{F})$ for all proper orthogonal \mathbf{Q} . It follows that $W(\mathbf{F}) = w(\mathbf{C})$, where

$$\mathbf{C} = \mathbf{F}^T \mathbf{F} = a_{\alpha\beta} \mathbf{A}^\alpha \otimes \mathbf{A}^\beta \quad (3.12)$$

is the Cauchy-Green strain. If w is symmetrized in the $a_{\alpha\beta}$, we find

$$\mathbf{T}^\alpha = J \sigma^{\alpha\beta} \mathbf{a}_\beta, \quad (3.13)$$

where

$$J = (a/A)^{\frac{1}{2}} \quad (3.14)$$

is the areal stretch, and

$$\sigma^{\alpha\beta} = 2J^{-1} \partial w / \partial a_{\alpha\beta} \quad (3.15)$$

are the contravariant components of the Cauchy stress

$$\boldsymbol{\sigma} = \sigma^{\alpha\beta} \mathbf{a}_\alpha \otimes \mathbf{a}_\beta. \quad (3.16)$$

Suppose the domain S has piecewise smooth boundaries, and the network is subjected to loads derivable from a potential $PT[\mathbf{r}]$, then we define a potential energy $E[\mathbf{r}]$ of the deformation by

$$E[\mathbf{r}] = \int_S W(\mathbf{F}) A^{1/2} d\theta^1 d\theta^2 - PT[\mathbf{r}]. \quad (3.17)$$

The equilibrium equations for the networks are the Euler-Lagrange equations associated with the functional E. For the problem of pressure load and concentrated load, these are

$$A^{-\frac{1}{2}}(A^{\frac{1}{2}}\mathbf{T}^\alpha), \alpha + pJ\mathbf{n} + \mathbf{P}\delta(\theta^1, \theta^2) = \mathbf{0}, \quad (3.18)$$

where p is the pressure value, \mathbf{P} is the concentrated load at point (θ^1, θ^2) , and \mathbf{T} is the Piola stress. Suppose the network is composed of two families of fibers, and each point at the reference surface has unit vectors \mathbf{L} and \mathbf{M} tangential to the fibres. At the corresponding point at the deformed surface, \mathbf{l} and \mathbf{m} are unit tangents to the fibres. They are related by

$$\lambda \mathbf{l} = \mathbf{F}\mathbf{L}, \quad \mu \mathbf{m} = \mathbf{F}\mathbf{M}, \quad (3.19)$$

where

$$\lambda = |\mathbf{F}\mathbf{L}|, \quad \mu = |\mathbf{F}\mathbf{M}| \quad (3.20)$$

are the fiber stretches. From the representations

$$\mathbf{l} = l^\alpha \mathbf{a}_\alpha, \quad \mathbf{m} = m^\alpha \mathbf{a}_\alpha, \quad (3.21)$$

we find

$$\lambda l^\alpha = L^\alpha, \quad \mu m^\alpha = M^\alpha. \quad (3.22)$$

We postulate that the force carried by the fiber of one family is independent of the stretch of the fiber in the other family. Then the strain energy of an elastic net can be expressed in the form

$$W = F(\lambda) + G(\mu), \quad (3.23)$$

where

$$\lambda^2 = \mathbf{L} \cdot \mathbf{C}\mathbf{L} = a_{\alpha\beta} L^\alpha L^\beta, \quad \mu^2 = \mathbf{M} \cdot \mathbf{C}\mathbf{M} = a_{\alpha\beta} M^\alpha M^\beta. \quad (3.24)$$

The stress is obtained from equations (3.15), (3.23) and (3.24):

$$J\sigma^{\alpha\beta} = \lambda^{-1}f(\lambda)L^\alpha L^\beta + \mu^{-1}g(\mu)M^\alpha M^\beta, \quad (3.25)$$

where

$$f(\lambda) = F'(\lambda), g(\mu) = G'(\mu) \quad (3.26)$$

are fiber stresses. We assume that $f(\lambda)$ and $g(\mu)$ are continuous. From (3.13), (3.21) and (3.22), we get

$$\mathbf{T}^\alpha = f(\lambda)\mathbf{l}L^\alpha + g(\mu)\mathbf{m}M^\alpha. \quad (3.27)$$

Then the Piola stress is

$$\mathbf{T} = f(\lambda)\mathbf{l} \otimes \mathbf{L} + g(\mu)\mathbf{m} \otimes \mathbf{M}. \quad (3.28)$$

If the network is composed of more than two families of fibers, for example N , they are arranged along $\mathbf{L}^1, \mathbf{L}^2, \dots, \mathbf{L}^N$ respectively. After deformation, the directions of fibers are changed to $\mathbf{l}^1, \mathbf{l}^2, \dots, \mathbf{l}^N$ correspondingly. The fiber stresses are $f^1(\lambda^1), f^2(\lambda^2), \dots, f^N(\lambda^N)$, and $\lambda^1, \lambda^2, \dots, \lambda^N$ are fiber stretches. Similarly, we can get a Piola stress expression for N families of fiber networks,

$$\mathbf{T} = f^1(\lambda^1)\mathbf{l}^1 \otimes \mathbf{L}^1 + f^2(\lambda^2)\mathbf{l}^2 \otimes \mathbf{L}^2 + \dots + f^N(\lambda^N)\mathbf{l}^N \otimes \mathbf{L}^N. \quad (3.29)$$

Chapter 4. Plane Reference Configuration

The flat reference configurations are bounded in a region Ω with a piecewise smooth boundary $\partial\Omega$. The position of a point in Ω with coordinates (x_1, x_2) is given by $\mathbf{x} = x_\alpha \mathbf{e}_\alpha$, $\alpha = 1, 2$, and is displaced to the point $\mathbf{r}(\mathbf{x}) = r_i(\mathbf{x}) \mathbf{e}_i$, where $i = 1, 2, 3$. Using Cartesian coordinates, and simplifying the results of the last chapter, we obtain $\mathbf{A}_1 = \mathbf{x}_{,1} = \mathbf{e}_1$, $\mathbf{A}_2 = \mathbf{x}_{,2} = \mathbf{e}_2$, $A_{\alpha\beta} = \delta_{\alpha\beta}$, $A = 1$. Therefore the equilibrium equations are

$$\text{div} \mathbf{T}(\mathbf{x}) + pJ\mathbf{n}(\mathbf{x}) + \mathbf{P}\delta(x_{o1}, x_{o2}) = \mathbf{0}, \quad (4.1)$$

where

$$J\mathbf{n} = \lambda\mu \mathbf{l} \times \mathbf{m}. \quad (4.2)$$

To prove this, suppose the angle between \mathbf{l}, \mathbf{m} is γ . With $\Delta = \mathbf{L} \otimes \mathbf{L} + \mathbf{M} \otimes \mathbf{M}$, we have

$$\mathbf{F} = \mathbf{F}\Delta = \mathbf{F}\mathbf{L} \otimes \mathbf{L} + \mathbf{F}\mathbf{M} \otimes \mathbf{M}. \quad (4.3)$$

Then

$$\mathbf{F} = \lambda \mathbf{l} \otimes \mathbf{L} + \mu \mathbf{m} \otimes \mathbf{M}, \quad (4.4)$$

the strain is

$$\mathbf{C} = \lambda^2 \mathbf{L} \otimes \mathbf{L} + \mu^2 \mathbf{M} \otimes \mathbf{M} + \lambda\mu \cos\gamma (\mathbf{L} \otimes \mathbf{M} + \mathbf{M} \otimes \mathbf{L}), \quad (4.5)$$

and the metric is

$$a_{\alpha\beta} = \lambda^2 L_\alpha L_\beta + \mu^2 M_\alpha M_\beta + \lambda\mu \cos\gamma (L_\alpha M_\beta + M_\alpha L_\beta). \quad (4.6)$$

Therefore $a = \det(a_{\alpha\beta}) = \lambda^2 \mu^2 \sin^2 \gamma$, $J = (a/A)^{1/2} = \lambda\mu \sin \gamma$, and $\mathbf{n} = \mathbf{l} \times \mathbf{m} / \sin \gamma$. Hence $J\mathbf{n} = \lambda\mu \mathbf{l} \times \mathbf{m}$.

The Piola stress in component form is the following:

$$T_{i\alpha} = f(\lambda) l_i L_\alpha + g(\mu) m_i M_\alpha, \quad (4.7)$$

\mathbf{F} , \mathbf{l} , \mathbf{m} in component form are

$$F_{i\alpha} = r_{i,\alpha} \quad (4.8)$$

$$l_i = \lambda^{-1} F_{i\alpha} L_\alpha; \quad m_i = \mu^{-1} F_{i\alpha} M_\alpha. \quad (4.9)$$

It is similar for cases with more than two families of fibers. Before discretizing, the equilibrium equations can be rewritten in DR form as:

$$\rho(\mathbf{x})\ddot{\mathbf{r}}(\mathbf{x}, t) + c\rho(\mathbf{x})\dot{\mathbf{r}}(\mathbf{x}, t) - \text{div}\mathbf{T}(\mathbf{x}, t) - pJ\mathbf{n}(\mathbf{x}, t) - \mathbf{P}\delta(x_{o1}, x_{o2}) = \mathbf{0}. \quad (4.10)$$

In order to nondimensionalize the DR equations, let ρ_0, a_0 and E_0 be representative density, length, and Young's Modulus respectively, so that

$$\mathbf{x} = a_0\bar{\mathbf{x}}, \quad \mathbf{r} = a_0\bar{\mathbf{r}}, \quad E = E_0\bar{E}, \quad \rho = \rho_0\bar{\rho},$$

$$T_{i\alpha} = E_0\bar{T}_{i\alpha}, \quad p = E_0a_0^{-1}\bar{p}, \quad c = \sqrt{\frac{E_0}{\rho_0a_0^2}}\bar{c},$$

$$\mathbf{P}\delta(x_{o1}, x_{o2}) = E_0a_0^{-1}\bar{\mathbf{P}}\delta(x_{o1}, x_{o2}), \quad \dot{\mathbf{r}} = a_0\frac{d\bar{\mathbf{r}}}{dt},$$

$$\ddot{\mathbf{r}} = \frac{d\dot{\mathbf{r}}}{dt} = a_0\frac{d^2\bar{\mathbf{r}}}{dt^2}, \quad t = \sqrt{\frac{\rho_0a_0^2}{E_0}}\bar{t}.$$

$\bar{\mathbf{x}}, \bar{\mathbf{r}}, \bar{E}, \bar{\rho}, \bar{t}, \bar{c}, \bar{p}, \bar{\mathbf{P}}\delta(x_{o1}, x_{o2})$ are dimensionless variables. Note that the dimensions of E are $(force)(length)^{-1}$ and the dimensions of c are $(time)^{-1}$. Substituting these into the DR equations, and performing simple algebraic operations, we get dimensionless DR equations which have the same form as the dimensional ones. For convenience, from now on, we delete the bars over the dimensionless variables.

We first discretize the partial differential DR equations in space domain and then change them into ordinary differential equations. As shown in Fig.5, each mesh node is labelled by a pair of integer superscripts (i, j) , the summation convention is not used for superscripts in this chapter and Chapter 4. The quadrilateral regions formed by the four nearest neighbours of each of the nodes are called zones and are indicated by closed arrows. Points on the arrow sides of such a quadrilateral are labelled by half-integer indices, and they are called zone-centred points. The stress, deformation gradient, and mass density are associated with the zone-centred points; the displacement, velocity, acceleration and the divergence of the stress are associated with the nodes. To approximate the divergence of the Piola stress at node (i, j) and

time step n , we use the conservative finite difference formulae in chapter two, with $\phi = T_{i\alpha}(\mathbf{x}, t_n)$ within the arrow contour. Thus

$$\begin{aligned}
2A^{i,j}(T_{i\alpha,\alpha})^{i,j,n} &= e_{\alpha\beta} \\
&[T_{i\alpha}^{i+1/2,j+1/2,n}(x_{\beta}^{i,j+1} - x_{\beta}^{i+1,j}) \\
&+ T_{i\alpha}^{i-1/2,j+1/2,n}(x_{\beta}^{i-1,j} - x_{\beta}^{i,j+1}) \\
&+ T_{i\alpha}^{i-1/2,j-1/2,n}(x_{\beta}^{i,j-1} - x_{\beta}^{i-1,j}) \\
&- T_{i\alpha}^{i+1/2,j-1/2,n}(x_{\beta}^{i,j-1} - x_{\beta}^{i+1,j})],
\end{aligned} \tag{4.11}$$

where $A^{i,j}$ is the half area of enclosed arrow quadrilateral,

$$\begin{aligned}
A^{i,j} &= \frac{1}{4}[(x_2^{i-1,j} - x_2^{i+1,j})(x_1^{i,j+1} - x_1^{i,j-1}) \\
&- (x_1^{i-1,j} - x_1^{i+1,j})(x_2^{i,j+1} - x_2^{i,j-1})].
\end{aligned} \tag{4.12}$$

Similarly, the deformation gradient $F_{i\alpha}^{i+1/2,j+1/2}$ within the mesh cell quadrilateral, in which the zone-centred point $(i + 1/2, j + 1/2)$ is at the center, is approximated by

$$\begin{aligned}
F_{i\alpha}^{i+1/2,j+1/2,n} &= (2A^{i+1/2,j+1/2})^{-1} e_{\alpha\beta} \\
&[(x_{\beta}^{i,j+1} - x_{\beta}^{i+1,j})(r_i^{i+1,j+1,n} - r_i^{i,j,n}) \\
&- (x_{\beta}^{i+1,j+1} - x_{\beta}^{i,j})(r_i^{i,j+1,n} - r_i^{i+1,j,n})],
\end{aligned} \tag{4.13}$$

where,

$$\begin{aligned}
A^{i+1/2,j+1/2} &= \frac{1}{2}[(x_2^{i,j+1} - x_2^{i+1,j})(x_1^{i+1,j+1} - x_1^{i,j}) \\
&- (x_1^{i,j+1} - x_1^{i+1,j})(x_2^{i+1,j+1} - x_2^{i,j})].
\end{aligned} \tag{4.14}$$

By integrating over a zone with node (i, j) , we have

$$m^{i,j} \ddot{\mathbf{r}}^{i,j,n} + cm^{i,j} \dot{\mathbf{r}}^{i,j,n} = \mathbf{p}^{i,j,n}, \tag{4.15}$$

where $(p^{i,j,n})_i = \mathbf{e}_i \cdot \mathbf{p}^{i,j,n} = A^{i,j}(T_{i\alpha,\alpha})^{i,j,n} + pJn_i^{i,j} + P_i^{i,j}$, and $m^{i,j} = \rho^{i,j}A^{i,j}$ is the nodal mass.

We can now use the DR iterative formulae in Chapter Two. In the following, we conclude the computing steps:

1. Initializing conditions and boundary conditions;
2. approximating deformation gradient at zone-centred points;
3. calculating $\lambda, \mu, \mathbf{l}, \mathbf{m}, \mathbf{n}$;
4. calculating fiber stresses $f(\lambda), g(\mu)$ with sublayer model;
5. calculating p_i ;
6. using DR iterative formulae.

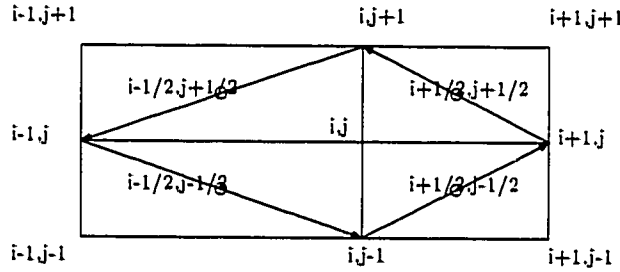


Fig.5 Finite difference mesh

For non-linear algebraic equations, we cannot give analytical proof of the DR stability, so before we use this scheme for computation, we do a numerical test of the stability of DR. If we choose a friction factor $c = 0$, then the system is conservative, so that the total mechanical energy (the sum of the potential energy and dynamic energy) should be constant. We tried it for a mesh size of 15×15 , and mesh size of 21×21 , with a time interval of 0 to 10^5 , we found that the total energies for the two mesh cases were constant and almost equal. Hence the stability of this numerical method is partly guaranteed.

The following are some numerical examples. The convergence condition of DR iteration is $0.1e-5$.

A. Static Case

(a) Linear Elastic Cases

Example 1

Specifications: (1) unit square domain, two family fibres, along x, y axis respectively; (2) fixed boundary, concentrated load $\mathbf{P}=(0,0,0.2)$ at center point.

The shape is shown in Fig.6. Fig.7 shows the shape with a pressure of 0.4 and $\mathbf{P}=(0,0,-0.2)$.

Example 2

Specifications: (1) unit circle domain; (2) pressure $upd=0.4$, concentrated load $\mathbf{P}=(0,0,-0.2)$ at center point, fixed boundary.

When two family fibres are along x and y axes respectively, the shape is shown in Fig.8; when the fibres are in radial and circular directions the shape is shown in Fig.9. We can find that Fig.8 is not axisymmetric, but Fig.9 is.

Example 3

Specifications: (1) triangle domain, two family fibres, along x, y axis respectively; (2) fixed boundary, pressure $upd=0.4$, $\mathbf{P}=(0,0,-0.2)$ at point (0,0).

The mesh is shown in Fig.10. The deformed shape is shown in Fig.11.

Example 4

Specifications: (1) ellipse domain, the long axis is 1.4, the short axis is 0.6; (2) fixed boundary, uniform pressure $upd=0.4$.

The mesh is shown in Fig.12. Fig.13 shows the deformed shape for the case in which the fibres are in x and y axial directions respectively; Fig.14 is for the case in which the fibres are in radial and circular directions respectively.

Example 5

Specifications: (1) L-domain, two family fibres are along x, y axis respectively; (2) fixed boundary, uniform pressure $upd=0.4$.

Fig.15 shows three different meshes. Fig.16 shows the deformed shapes corresponding to meshes in Fig.15.

Example 6

Specifications: (1) unit square domain, four family fibres in 0° , 45° , 90° , 135° directions respectively; (2) $y=-0.5$ and $y=0.5$ free, $x=-0.5$ and $x=0.5$ are fixed; (3) $x=0.5$ moves to 1.0; (4) uniform mesh 21×21 .

If the fibres can sustain the compressive stress, the deformed shape is shown in Fig.17. When we compute this case, if we set all node mass as equal, say $m = 1.1$, the results are very poor; if we reduce the node masses at free boundaries by half, $m = 1.1/2$, the results are good. When uniform stretching force $sforce = 1.0$ is applied at $x=0.5$, mesh 21×21 , the shape is shown in Fig.17a. When we suppose that the fibres can sustain only tensile stresses, the shape with wrinkles is shown in Fig.18. The wrinkled zones are marked by '+'.

Example 7

Specifications: (1) the same as (1) in Example 6; (2) only four corners are fixed; (3) the 4 corners stretch out a distance of $0.2\sqrt{2}$.

A quarter of the deformed shape is shown in Fig.19. When it is subjected to uniform pressure $upd=0.1$, the shape is shown in Fig.20. The wrinkled zones are marked by '+'.

(b) Elastic Plastic Cases

With the two sublayer model, the stress-strain relationship is composed of three straight line segments. The first segment is from (0,0) to (0.15,0.15), the second one is from (0.15,0.15) to (7,18), and the third one is from (7,18) to (7,infinity).

The wrinkled zones are marked by '+'.

Example 1

Specifications: unit square domain, two family fibres along x and y axes respectively.

When uniform pressure increases from 0 to 0.8, the shape is shown in Fig.21; when the pressure decreases to 0, the shape is shown in Fig.22. The relationship between the mid point displacement and the uniform pressure is shown in Fig.23.

Example 2

Specifications: unit circle domain, two family fibres are in radial and circular directions.

When uniform pressure increases from 0 to 0.3, the shape is shown in Fig.24; when it decreases from 0.3 to 0, the shape is shown in Fig.25. The relationship between the mid point displacement and the uniform pressure is shown in Fig.26.

Example 3

Specifications: (1) unit square domain, three family fibres at 0° , 45° , 135° ; (2) $x=-0.5$ is fixed, $y=0.5$ and $y=-0.5$ and freedoms of x direction at $x=0.5$ are free.

When the stretching force in x -direction at $x=0.5$ increases from 0 to 0.4, the shape is shown in Fig.27; when the stretching force decreases from 0.4 to 0.05, the shape is shown in Fig.28.

Discussion

In the calculating process, some experience with choosing fictitious density or mass is gained. Usually, for block iteration, the fictitious mass matrix is supposed to be constructed in order to get the best convergent speed as in Philip [1983]. For point iteration, we do not need to construct matrices, so the fictitious densities are supposed to be determined as in Cassel [1970]. As point iteration is used, for simplicity, we choose uniform and isotropic fictitious density, for uniform mesh. This works well. But for non-uniform mesh, the convergence is slow. In this case, we found that if we set all node masses $m = 1.1$, regardless of their corresponding mesh areas(it is as with a non-uniform fictitious density.), the convergent speed is 3 to 5 times faster.

From the above examples, it is clear that the Explicit Lagrangian Finite Difference is good at adapting to the different domains. The sublayer model is convenient when considering the elasticity and plasticity in the same formulae. For more than one concentrated load case, difficulty arises concerning how to generate the mesh.

B. Simulation of Punching

(a) Sudden Application of Force

Example 1

Specifications: (1) unit circle domain, two family fibres in radial and circular directions; (2) $\mathbf{P} = (0, 0, 0.2)$, the same el-pl sublayer model as the above; (3) $c=0.17$, density=2000.0; (4) at the position when velocity is zero.

Fig.29 shows the shape that is independent of strain rate; Fig.30 shows the shape that is dependent on strain rate by $\sigma_y = \sigma_0(1 + 5\dot{\epsilon})$. The strain rate effect is obvious.

(b) Punching Head With Speed $h_v(t)$

Example 1

Specifications: (1) unit circle domain, two family fibres in radial and circular directions; (2) elastic case, pre-tension $pt=0.4$; (3) $c=0.17$, density=2000.0; (4) h_v is the velocity of the punching head; (5) The radius of the punching head $rh=0.1667$.

Here we prove numerically that the static case is the limit of the infinitely slow loading case. When the head moves to 0.1, shapes at different velocities are shown. When $h_v=0.1$ the shape is shown in Fig.31. When $h_v=0.01$ the shape is shown in Fig.32. When $h_v=0.001$ the shape is shown in Fig.33. The trend approaching the static state is obvious. We can also notice that with an increase in pre-tension of fibers, the speed of disturbance transportation is also increased.

Example 2

Specifications: (1) unit circle domain, two family fibres in radial and circular directions; (2) elastic case, $rh=0.1667$; (3) $c=0.17$, density=2000.0; (4) $h_v=0.02$, where h_v is the velocity of the punching head, and there is no pre-tension.

To simulate the penetration, we set that when the stretch is 2.0, the fibre cannot sustain the stress. Fig.34 shows the shape when the head moves to 0.06; Fig.35 shows the shape when head moves to 0.4.

(c) Approximation Of Low Speed Punching With Static Stiffness.

Example 1

Specifications: (1) unit circle domain, two family fibres in radial and circular directions; (2) elastic case; (3) $c=0.17$, density=2000.0; (4) $h_v=0.02$, where h_v is the velocity of the punching head, and pre-tension $pt=0.2$; (5) a plane circular object with mass $um=3.0$, radius $rh=0.1$, velocity when touching the net, $udl=0.2$, time step $h=0.01$.

Approximation Procedures

Step one : We simplify the net as a spring, in order to get the stiffness k . We use the static method to get a series of mid point forces and mid point displacements (P_i, r_i) . Then use least-square recession to get the approximation function $P = a_1r + a_2r^2 + a_3r^3 + a_4r^4$. Then we can get $k = a_1 + 2a_2r + 3a_3r^2 + 4a_4r^3$. $k = a_1$ is the linear case.

Step two : With ICs $r = 0$, $\dot{r} = udl$, $t = 0$, we can get a numerical solution of $um\ddot{r} + c\dot{r} - kr = 0$.

Step three : The numerical solution of the spring mass system is the motion of the punching object after contact. So we can get the motion state of the net.

Fig.36 shows the static mid point force-displacement relationship.

Fig.37 shows the motion of the mass.

Fig.38 shows the shape when the impacting object reaches the maximum displacement position.

Discussion

When the s-s relation is strain rate dependent, it can influence the shape after the punching. It is important to consider the plasticity in impact problems, for the design of impact proof structures is based on the plasticity of the material to absorb the energy. Impact and penetration are very complicated phenomena; the examples here are simple and primary.

Chapter 5. Circular Cylinder Reference Configuration

The circular cylinder reference configuration has a height 1 and a radius $R = 1/2\pi$. The position of a point on the surface with cylindrical coordinates (θ, z) is given by $\mathbf{x} = R\mathbf{e}_r(\theta) + z\mathbf{k}$, and is displaced to the point $\mathbf{r}(\mathbf{x}) = (R + \Delta)\mathbf{e}_r(\theta) + R d\theta \mathbf{e}_\theta(\theta) + (z + dz)\mathbf{k}$. Simplifying the results in Chapter 3 with $x_1 = \theta$, and $x_2 = z$, we can get $\mathbf{A}_1 = \mathbf{x}_{,1} = R\mathbf{e}_\theta$, $\mathbf{A}_2 = \mathbf{x}_{,2} = \mathbf{k}$, $A = R^2$. The equilibrium equations are

$$\text{div} \mathbf{T}(\mathbf{x}) + pJ\mathbf{n}(\mathbf{x}) + \mathbf{P}\delta(x_{o1}, x_{o2}) = \mathbf{0}, \quad (5.1)$$

where

$$J\mathbf{n} = \lambda\mu \mathbf{l} \times \mathbf{m}, \quad (5.2)$$

$$\mathbf{T} = f(\lambda)\mathbf{l} \otimes \mathbf{L} + g(\mu)\mathbf{m} \otimes \mathbf{M}, \quad (5.3)$$

or in component form,

$$T_{i\alpha} = f(\lambda)l_i L_\alpha + g(\mu)m_i M_\alpha. \quad (5.4)$$

It is similar to the plane reference configuration case. The main difference is that here we use the Navier-Stokes' theorem instead of Green's theorem when we integrate the equations over the surface.

$$\int \int (\nabla \times \mathbf{u}) \cdot d\mathbf{A} = \int \mathbf{u} \cdot d\mathbf{s}, \quad (5.5)$$

where

$$\begin{aligned} \nabla \times \mathbf{u} &= \left(\frac{1}{r} \frac{\partial u_z}{\partial \theta} - \frac{\partial u_\theta}{\partial z} \right) \mathbf{e}_r \\ &\quad + \left(\frac{\partial u_r}{\partial z} - \frac{\partial u_z}{\partial r} \right) \mathbf{e}_\theta \\ &\quad + \frac{1}{r} \left(\frac{\partial(r u_\theta)}{\partial r} - \frac{\partial u_r}{\partial \theta} \right) \mathbf{k}, \\ \int \int (\nabla \times \mathbf{u}) \cdot d\mathbf{A} &= \int \int \left(\frac{1}{r} \frac{\partial u_z}{\partial \theta} - \frac{\partial u_\theta}{\partial z} \right) dA, \\ \int \mathbf{u} \cdot d\mathbf{s} &= \int u_\theta r d\theta + u_z dz. \end{aligned}$$

Let $u_z = \mathbf{T}_1$, $u_\theta = 0$ and $u_z = 0$, $u_\theta = \mathbf{T}_2$ separately, thus

$$\begin{aligned} \iint \operatorname{div} \mathbf{T} dA &= \iint \left(\frac{1}{r} \frac{\partial \mathbf{T}_1}{\partial \theta} + \frac{\partial \mathbf{T}_2}{\partial z} \right) dA \\ &= \int \mathbf{T}_1 dz - \mathbf{T}_2 R d\theta. \end{aligned} \quad (5.6)$$

Just as in the plane case, we integrate the DR equations over the cylinder surface with the mesh in Fig.5, and get

$$\begin{aligned} 2A^{i,j}(\operatorname{div} \mathbf{T})^{i,j,n} &= \\ &[T_{i1}^{i+1/2,j+1/2,n}(x_2^{i,j+1} - x_2^{i+1,j}) + T_{i1}^{i-1/2,j+1/2,n}(x_2^{i-1,j} - x_2^{i,j+1}) \\ &+ T_{i1}^{i-1/2,j-1/2,n}(x_2^{i,j-1} - x_2^{i-1,j}) - T_{i1}^{i+1/2,j-1/2,n}(x_2^{i,j-1} - x_2^{i+1,j})] - \\ &R[T_{i2}^{i+1/2,j+1/2,n}(x_1^{i,j+1} - x_1^{i+1,j}) + T_{i2}^{i-1/2,j+1/2,n}(x_1^{i-1,j} - x_1^{i,j+1}) \\ &+ T_{i2}^{i-1/2,j-1/2,n}(x_1^{i,j-1} - x_1^{i-1,j}) - T_{i2}^{i+1/2,j-1/2,n}(x_1^{i,j-1} - x_1^{i+1,j})], \end{aligned} \quad (5.7)$$

where half the area of the enclosed arrow quadrilateral is,

$$\begin{aligned} A^{i,j} &= \frac{R}{4} [(x_2^{i-1,j} - x_2^{i+1,j})(x_1^{i,j+1} - x_1^{i,j-1}) \\ &\quad - (x_1^{i-1,j} - x_1^{i+1,j})(x_2^{i,j+1} - x_2^{i,j-1})]. \end{aligned} \quad (5.8)$$

Similarly, for deformation gradient. For $F_{1\alpha}$,

$$\begin{aligned} F_{1\alpha}^{i+1/2,j+1/2,n} &= (2A^{i+1/2,j+1/2})^{-1} \\ &[(x_2^{i,j+1} - x_2^{i+1,j})(r_1^{i+1,j+1,n} - r_1^{i,j,n}) * (r_1^{i+1,j+1,n} + r_1^{i,j,n})/2 \\ &- (x_2^{i+1,j+1} - x_2^{i,j})(r_i^{i,j+1,n} - r_i^{i+1,j,n}) * (r_i^{i,j+1,n} - r_i^{i+1,j,n})/2] - \\ &R[(x_1^{i,j+1} - x_1^{i+1,j})(r_i^{i+1,j+1,n} - r_i^{i,j,n}) * (r_i^{i+1,j+1,n} - r_i^{i,j,n})/2 \\ &- (x_1^{i+1,j+1} - x_1^{i,j})(r_i^{i,j+1,n} - r_i^{i+1,j,n}) * (r_i^{i,j+1,n} - r_i^{i+1,j,n})/2]; \end{aligned} \quad (5.9)$$

for $F_{i\alpha}$, $i = 2, 3$

$$\begin{aligned} F_{i\alpha}^{i+1/2,j+1/2,n} &= (2A^{i+1/2,j+1/2})^{-1} \\ &[(x_2^{i,j+1} - x_2^{i+1,j})(r_i^{i+1,j+1,n} - r_i^{i,j,n}) \\ &- (x_2^{i+1,j+1} - x_2^{i,j})(r_i^{i,j+1,n} - r_i^{i+1,j,n})] - \\ &R[(x_1^{i,j+1} - x_1^{i+1,j})(r_i^{i+1,j+1,n} - r_i^{i,j,n}) \\ &- (x_1^{i+1,j+1} - x_1^{i,j})(r_i^{i,j+1,n} - r_i^{i+1,j,n})]. \end{aligned} \quad (5.10)$$

where,

$$A^{i+1/2,j+1/2} = \frac{R}{2}[(x_2^{i,j+1} - x_2^{i+1,j})(x_1^{i+1,j+1} - x_1^{i,j}) - (x_1^{i,j+1} - x_1^{i+1,j})(x_2^{i+1,j+1} - x_2^{i,j})]. \quad (5.11)$$

The rest of the formulae are the same as those in Chapter 4.

The following numerical examples are elastic cases with a convergence condition of DR iteration as $0.1e-5$.

Example 1

For comparison, first we calculate the unit square case. Two family fibres are in x, y directions respectively, with $x=-0.5$ and $x=0.5$ fixed; $y=-0.5$ and $y=0.5$ are free. With uniform pressure $upd=0.4$, the shape is shown in Fig.39; then with the two fixed sides coming together, the shape is shown in Fig.40.

Example 2

Specifications: (1) the domain is the surface of a circular cylinder, with height 1 and radius $1/2\pi$.

When $\theta = 0$ (or $\theta = 2\pi$) is fixed and the uniform pressure $upd=0.4$, the shape is shown in Fig.41. We can see the difference between Fig.41 and Fig.40. The results depend on the loading paths. When $z=0$ and $z=1$ are fixed, the shape is shown in Fig.42. When $z=1$ is fixed, and freedom in r direction at $z=0$ is free, uniform pressure $upd=0.1$. The shape is shown in Fig.43.

Example 3

Specifications: (1) the domain is the surface of a circular cylinder, with height 1 and radius $1/2\pi$.

When $upd=0.4$, with different meshes, the shape is shown in Fig.44. With an additional concentrated load $\mathbf{P} = (0, 0, -0.2)$, the shape is shown in Fig.45.

Discussion

The circular cylinder is only a special curve surface. For an arbitrary curve surface, there is no way to implement the Explicit Lagrangian Finite Difference formulae.

Chapter 6. Conclusions and Remarks

Explicit Lagrangian Finite Difference(ELFD) methods and Dynamic Relaxation(DR) have been used to solved some problems.

1. For various domains, ELDF shows its flexibility to discretize the domains and adapt the boundaries. In cases with one concentrated load applied, co-centered circuits and radiative segments can be generated to produce the mesh grids. The center is the point at which the concentrated load is applied. Only mesh nodes need to be recorded. The information concerning what nodes consist of which cell is automatically clear, and need not be recorded additionally. It is very easy to implement in programs. The pre-processing part is quite short. Theoretically, ELDF can be used in any kind of mesh grid if infomation about which cell has what nodes and which node has what neighbouring cells can be recorded. These things can be done, but it is very difficult to do so. The mature commercial Finite Element method softwares can deal with nearly any domain and any mesh grids.

2. When DR is used, the way to choose all node masses as 1.0, no matter whether the mesh grids are uniform or not, shows its advantages in many static numerical examples. It is a concept of non-unifrom fictitious density. It seems that non-uniform fictitious density has advantages over uniform fictitious density. Its mathematical proof is not available yet.

3. Impact and penetration are very difficult and complex; some of the work here is in the primary stage. The methods that have been adopted in this work are limited to low velocity cases.

4. The circular cylinder surface is only a specific and simple curved surface case. There are many similarities between a circular cylinder surface and a plane rectangle. The ELFD methods are easy to implement in the circular cylinder surface case. Numerical examples show that it works well. But for arbitrary curved reference surfaces, the ways to implement ELFD methods are not yet available. Though the shell membrane model is limited, the FEM

can be used to solve problems with any arbitrary curved surface. Geometrical shape is not a problem for FEM.

5. There is still a lot of work left to be done in networks. Analytical investigations are the basis for numerical investigations. Extra effort should be made on both aspects. The two important assumptions in this work are that the networks have no bending stiffness and that there is no slip between fibres on the crossing points. Future work may be done without taking into account one or the other of the above assumptions.

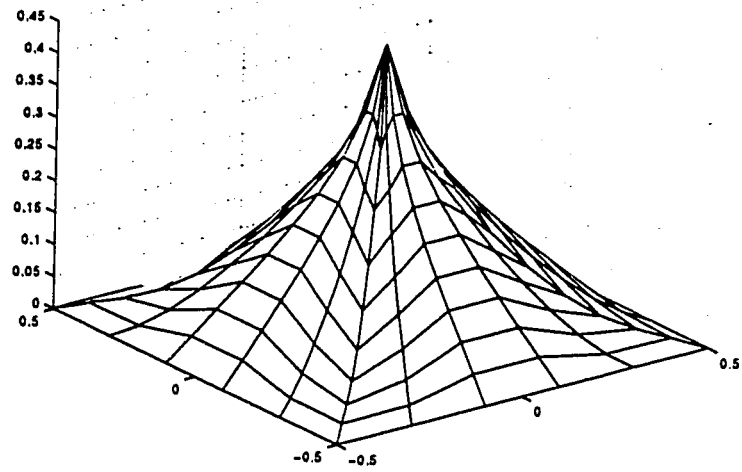


Figure 6: Shape with point load at center

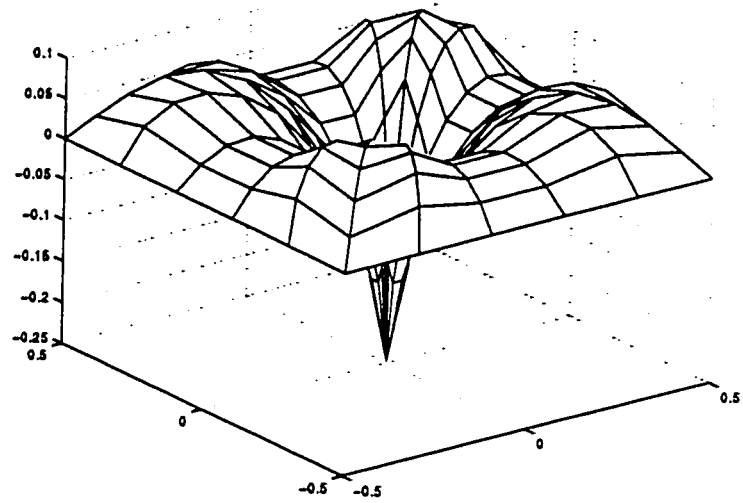


Figure 7: Shape with point load at center and pressure

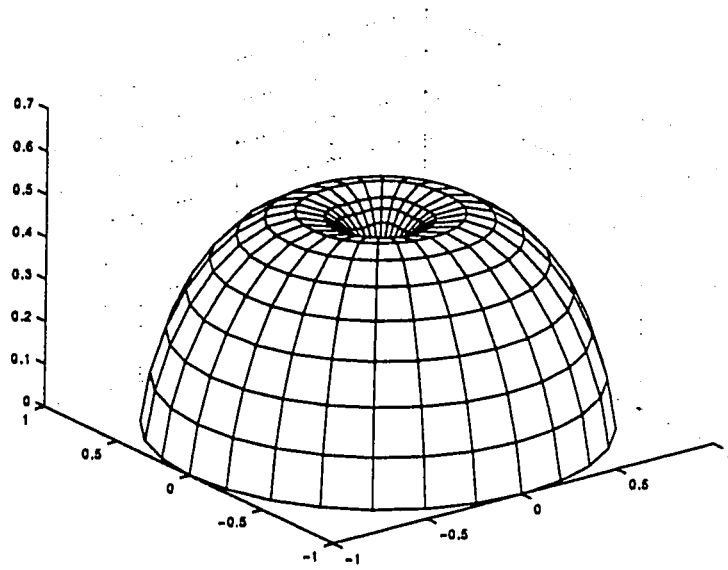


Figure 8: Shape with point load at center and pressure

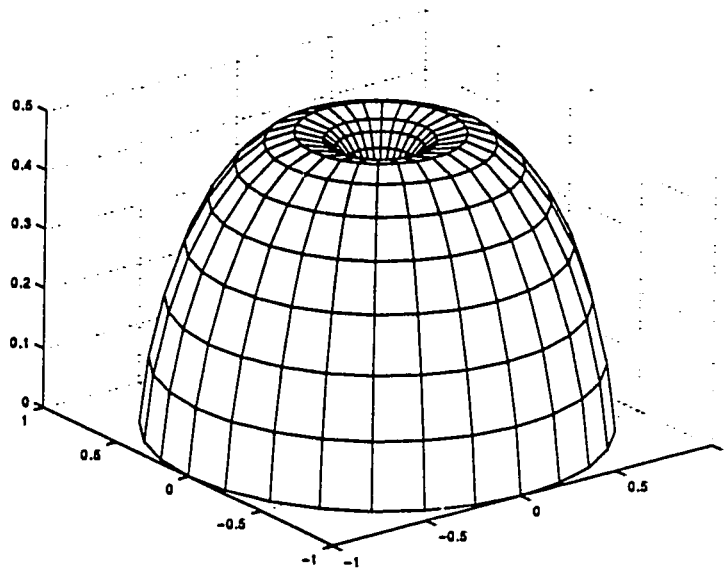


Figure 9: Deformed shape of circular network

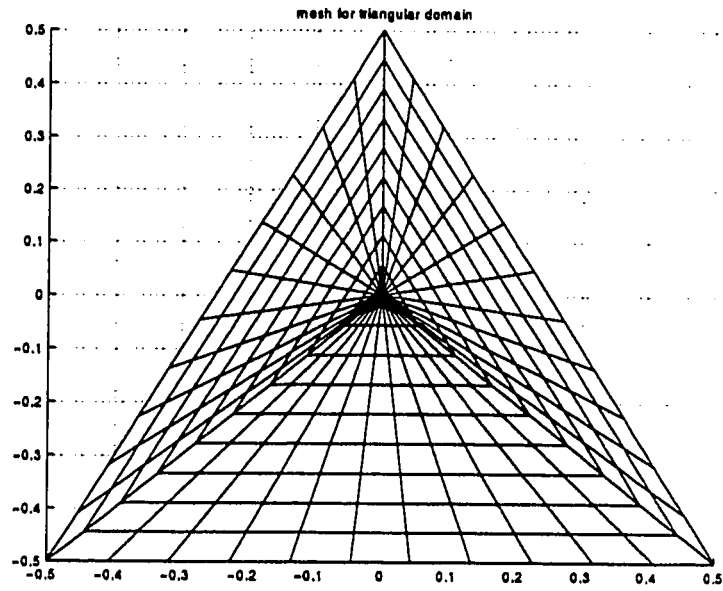


Figure 10: Mesh for triangular domain

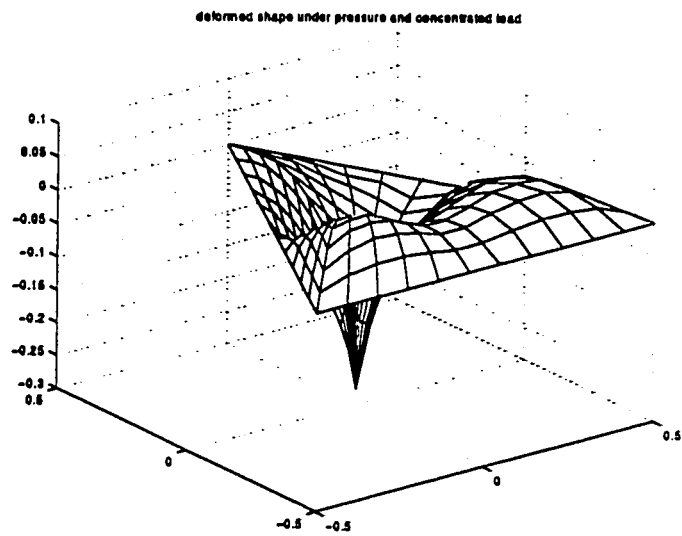


Figure 11: Deformed shape of triangle network

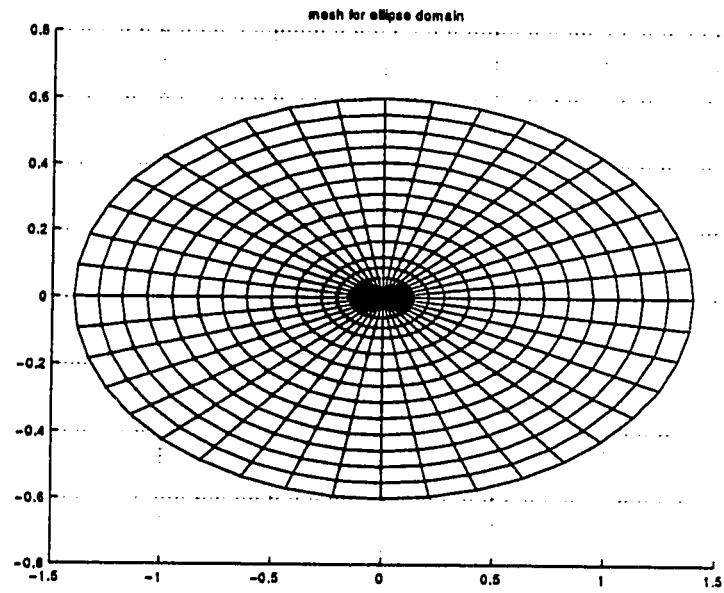


Figure 12: Mesh for ellipse domain

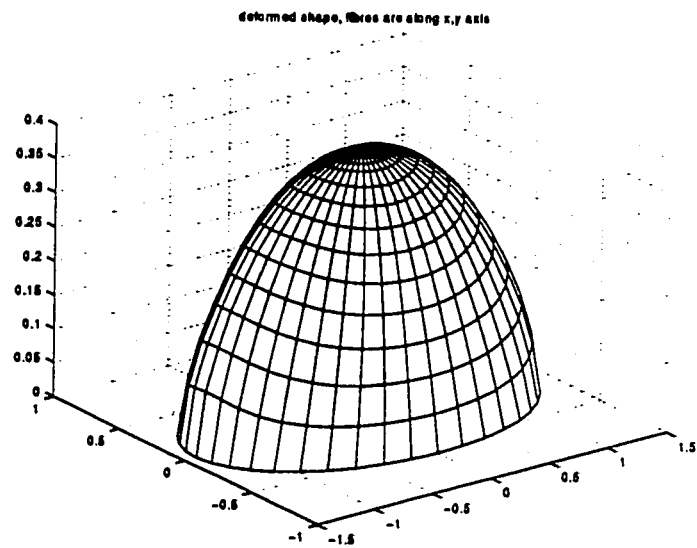


Figure 13: Deformed shape of ellipse network

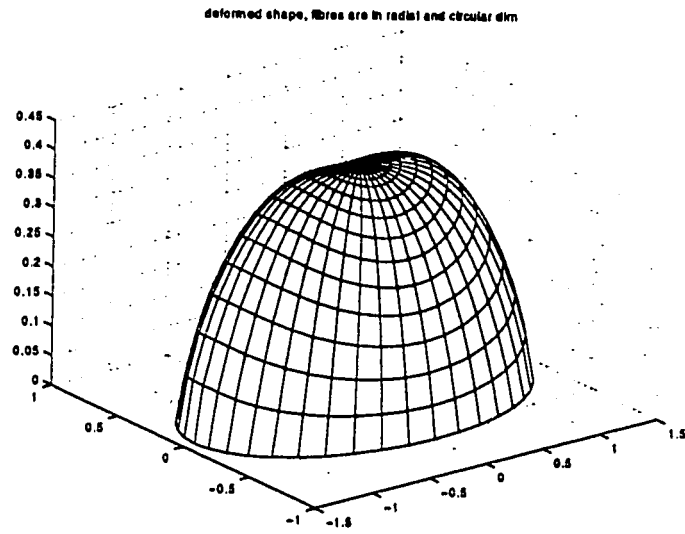


Figure 14: Deformed shape of ellipse network

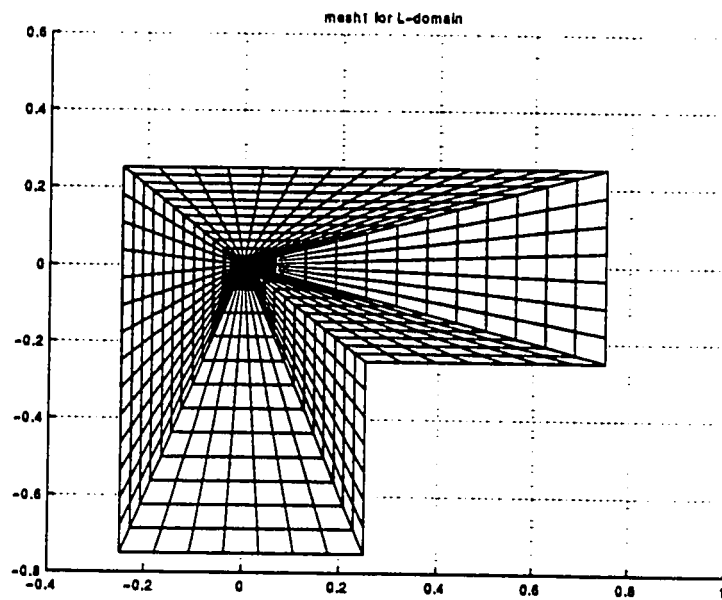


Figure 15a: Mesh one for L-domain

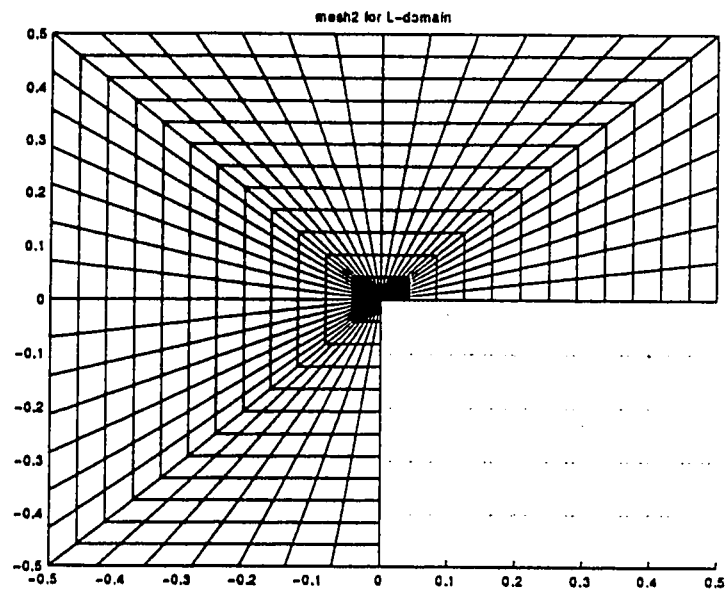


Figure 15b: Mesh two for L-domain

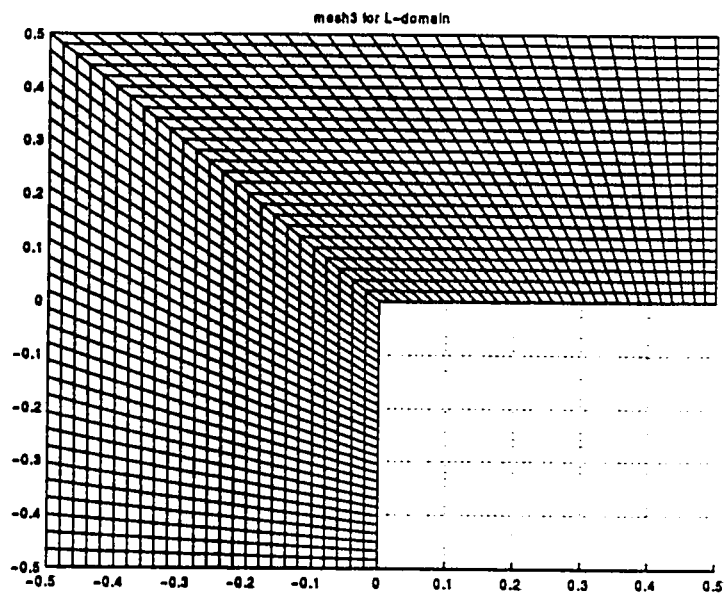


Figure 15c: Mesh three for L-domain

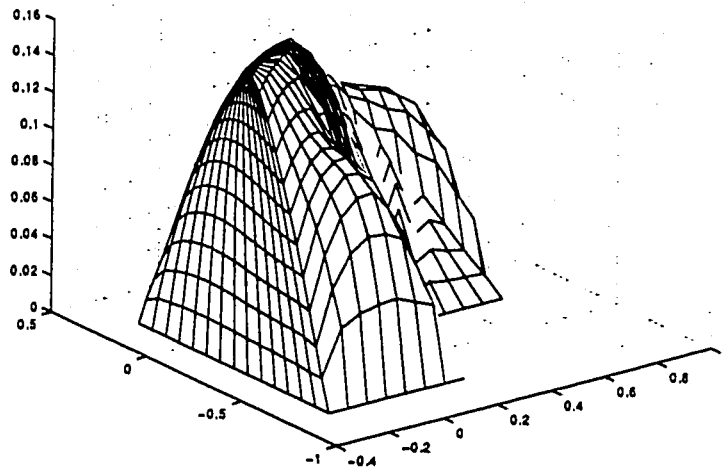


Figure 16a: Deformed shape with mesh 1

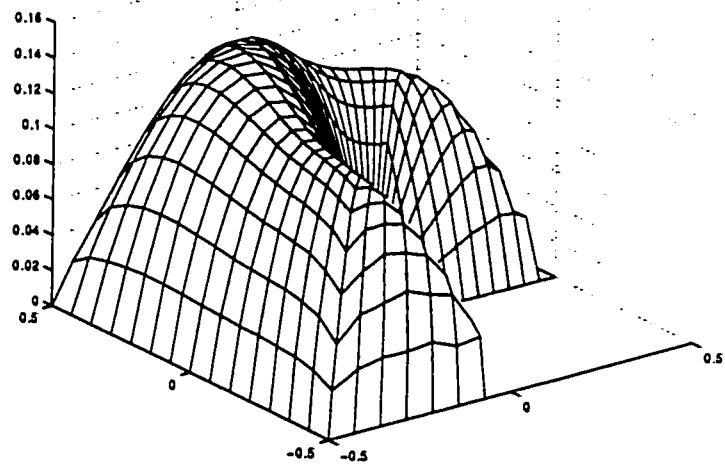


Figure 16c: Deformed shape with mesh 2

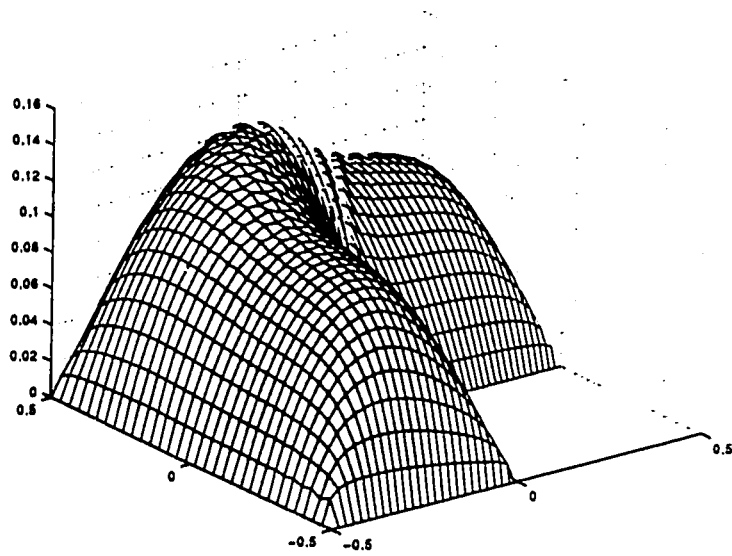


Figure 16c: Deformed shape with mesh 3

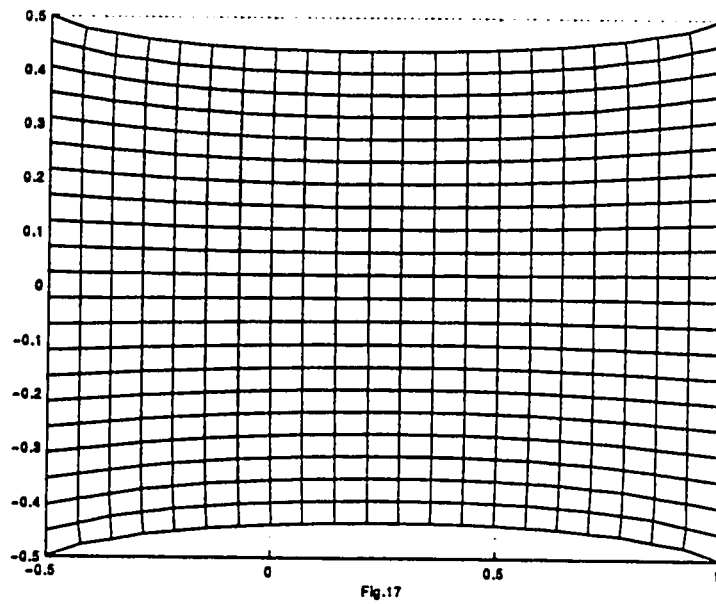


Figure 17: Deformed shape of 4-family fiber network

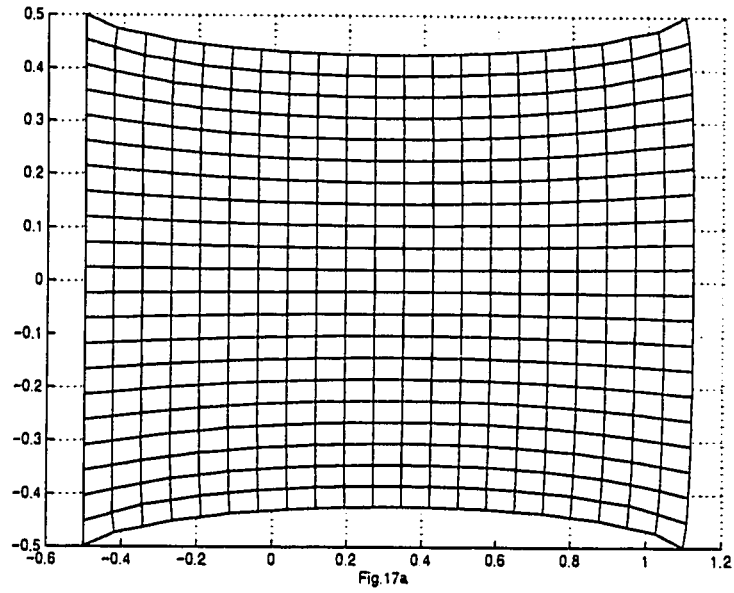


Figure 17a: Defromed shape after being stretched

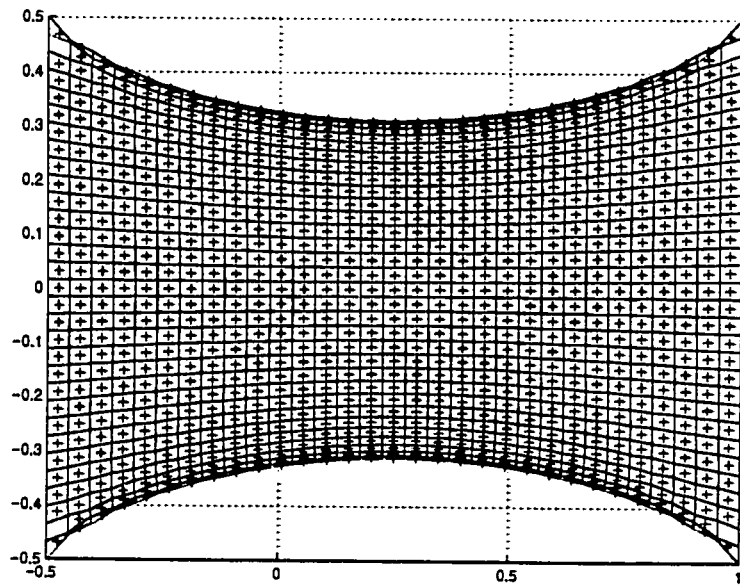


Figure 18: Deformed shape of 4-family fiber network

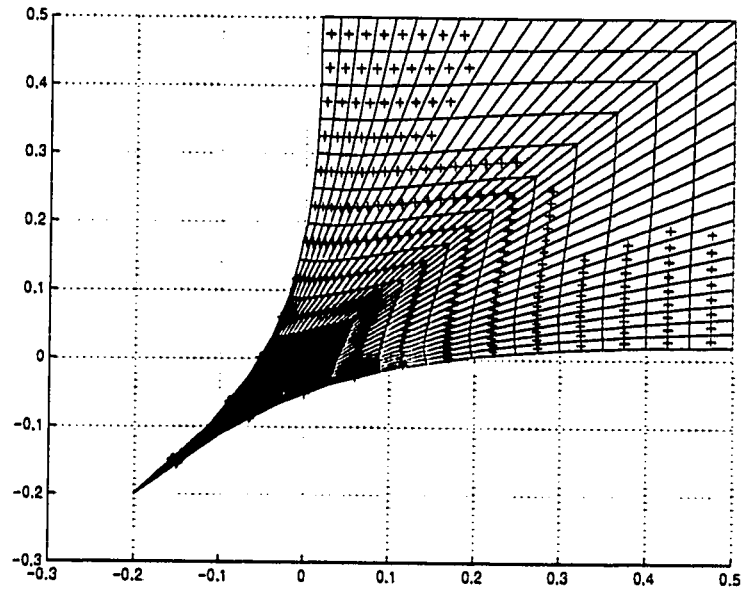


Figure 19: Deformed shape of unit square network

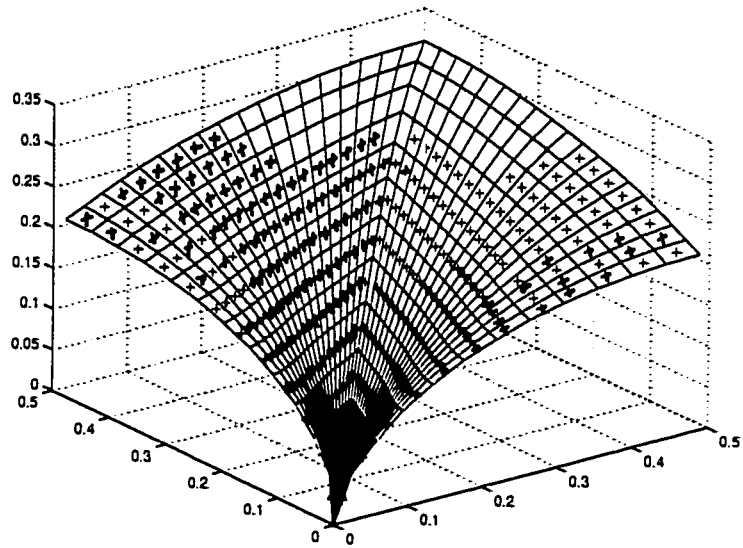


Figure 20: Deformed shape of unit square network

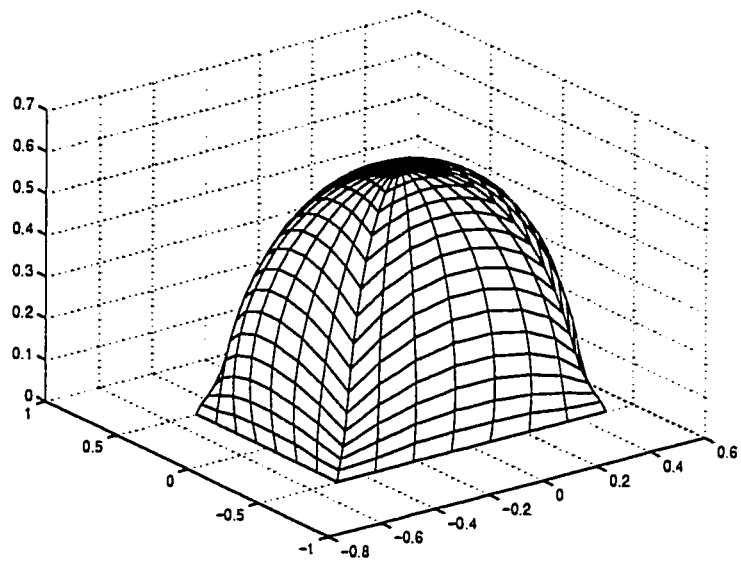


Figure 21: Deformed shape in plastic range

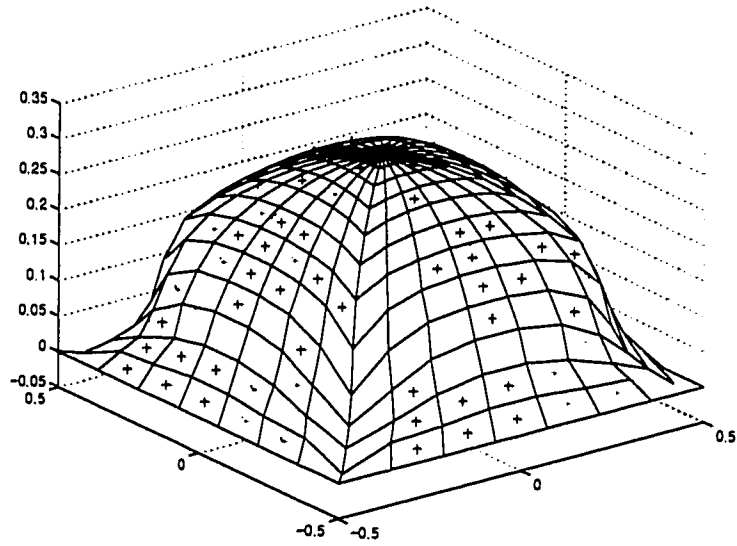


Figure 22: Residual shape after unloading

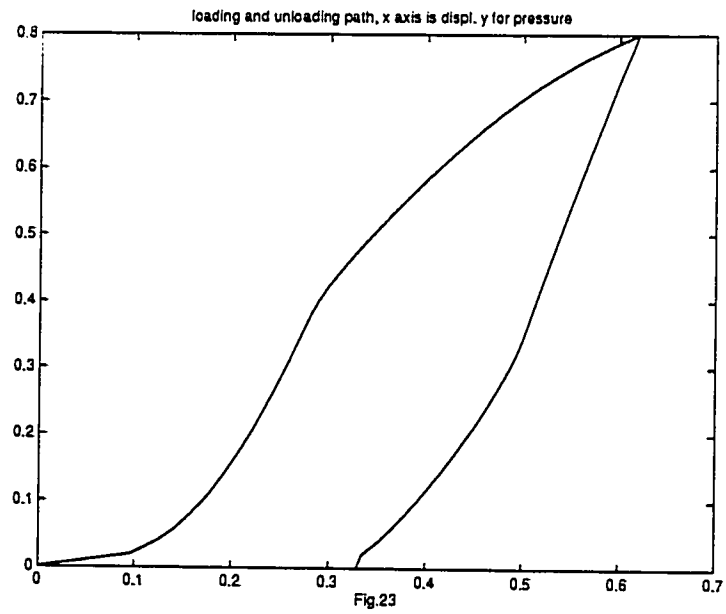


Figure 23: Load-displacement relationship

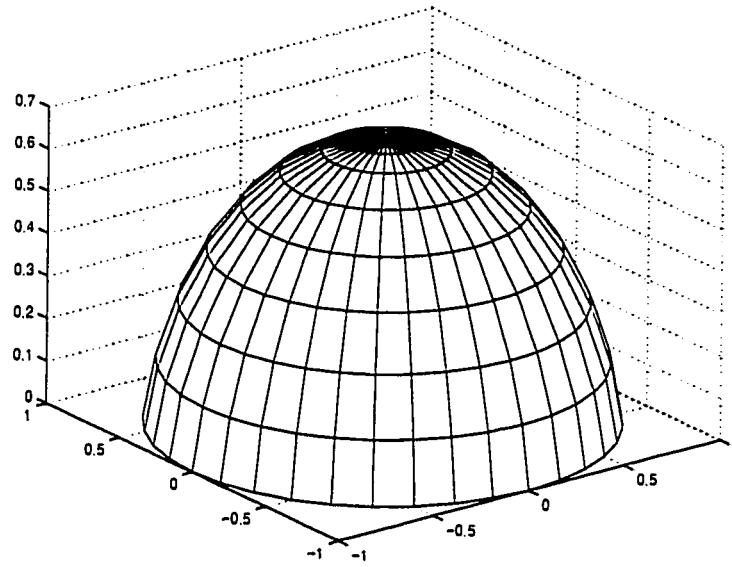


Figure 24: Deformed shape of unit circle network

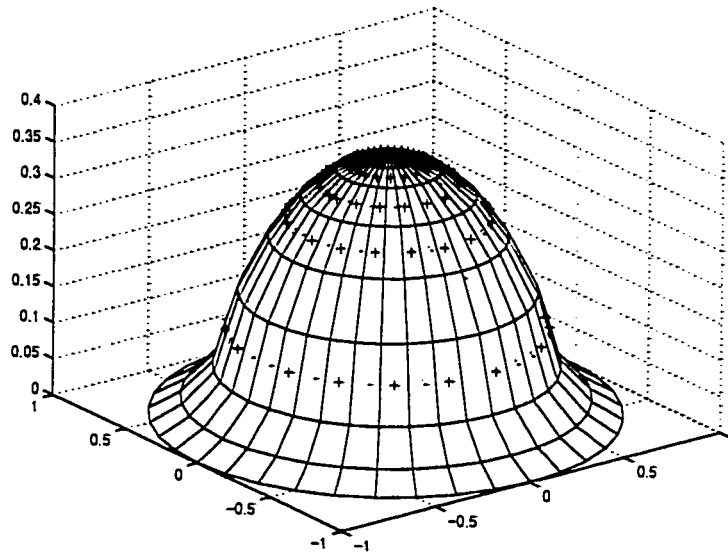


Figure 25: Residual shape of unit circle network

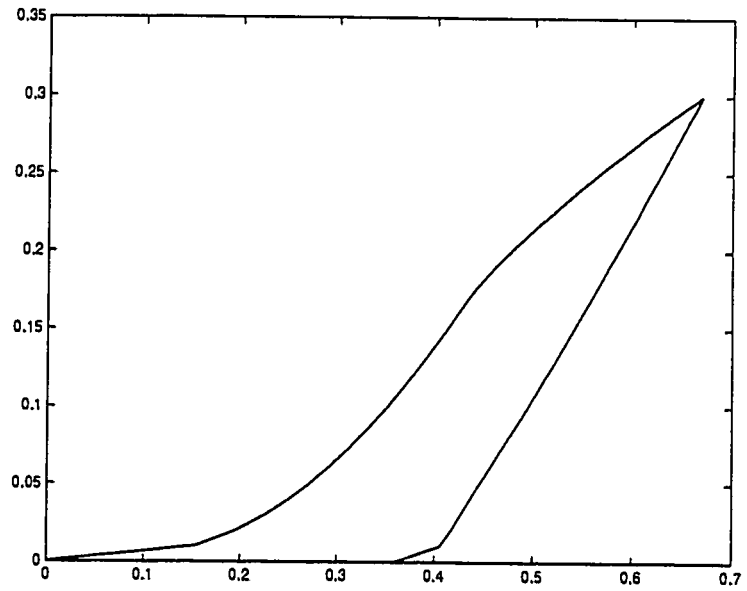


Figure 26: Load-displacement relationship

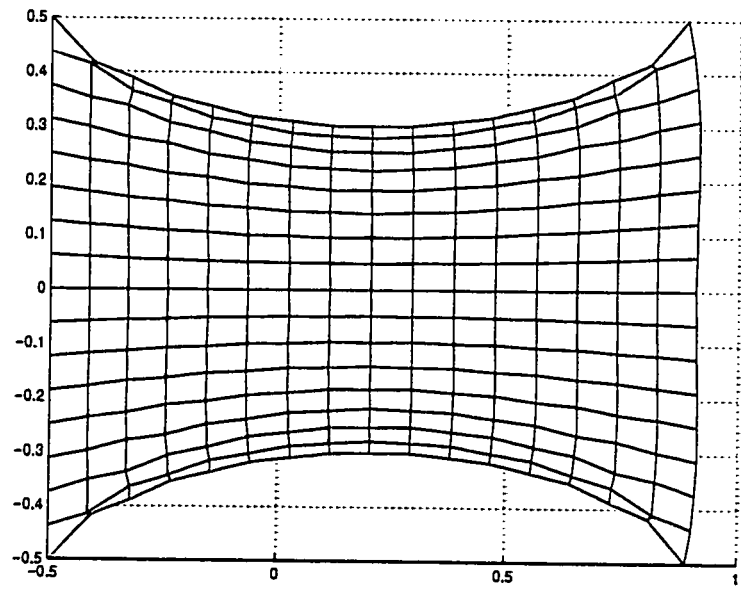


Figure 27: Deformed shape of unit square network

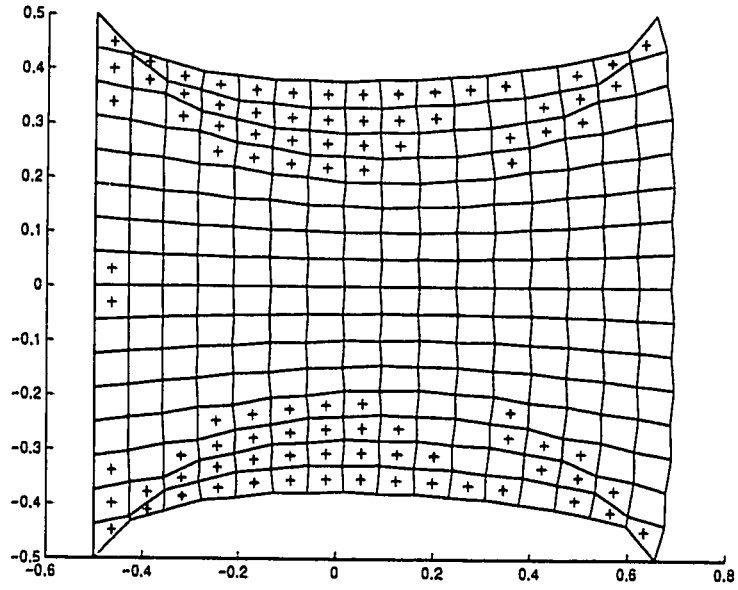


Figure 28: Deformed shape of unit square network after unloading

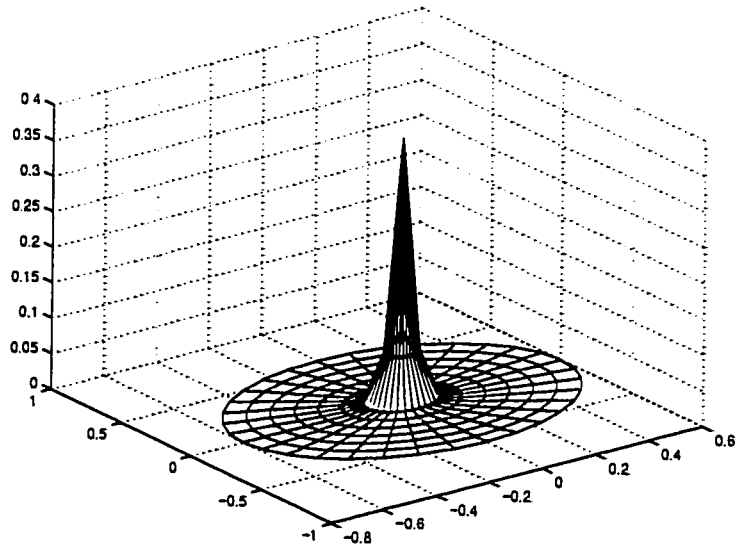


Figure 29: Deformed shape independent of strain rate

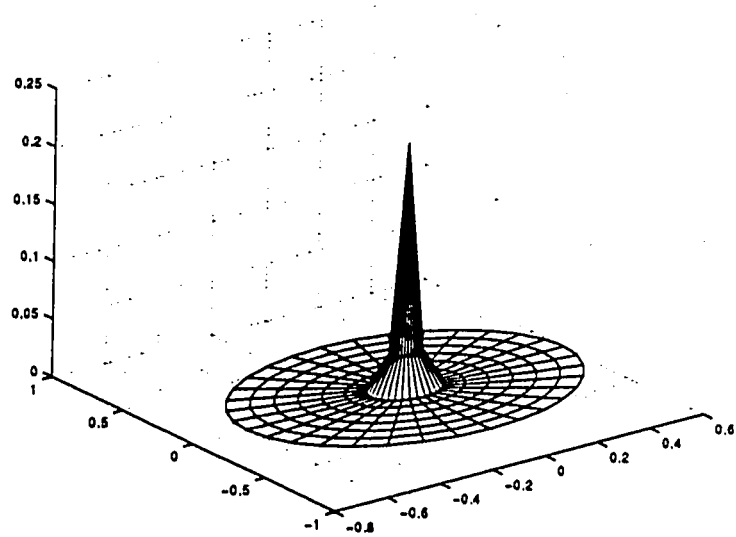


Figure 30: Deformed shape dependent of strain rate

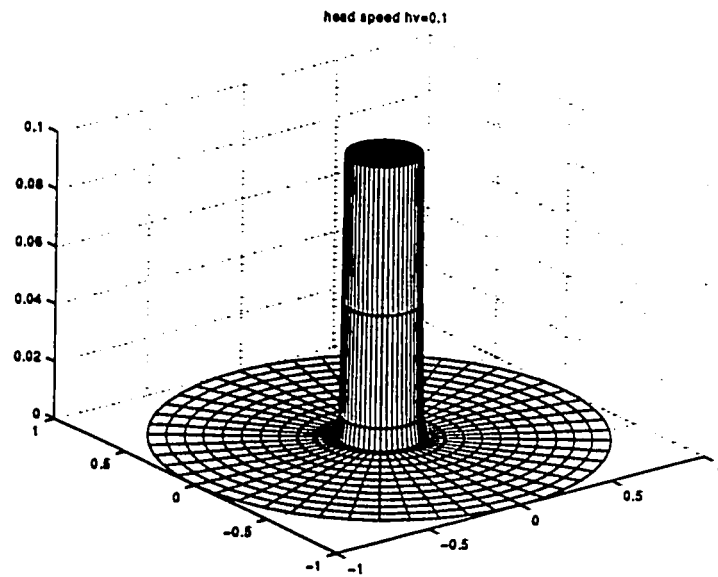


Figure 31: Deformed shape when $h\nu=0.1$

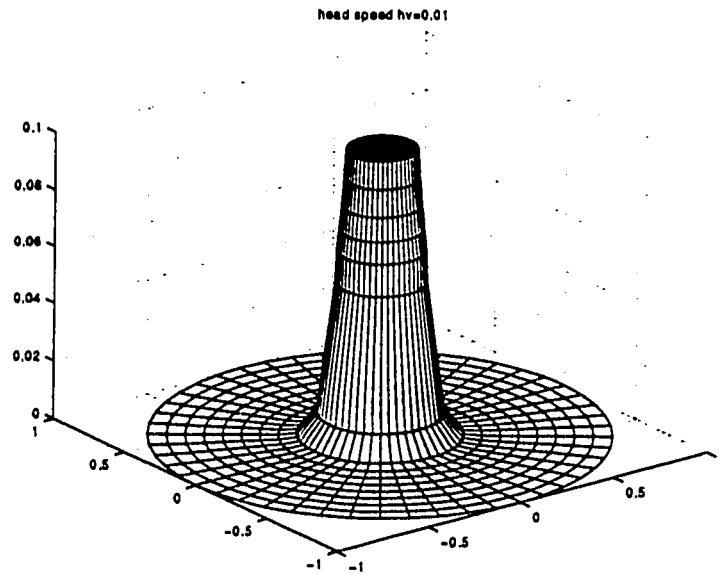


Figure 32: Deformed shape when $h\nu=0.01$

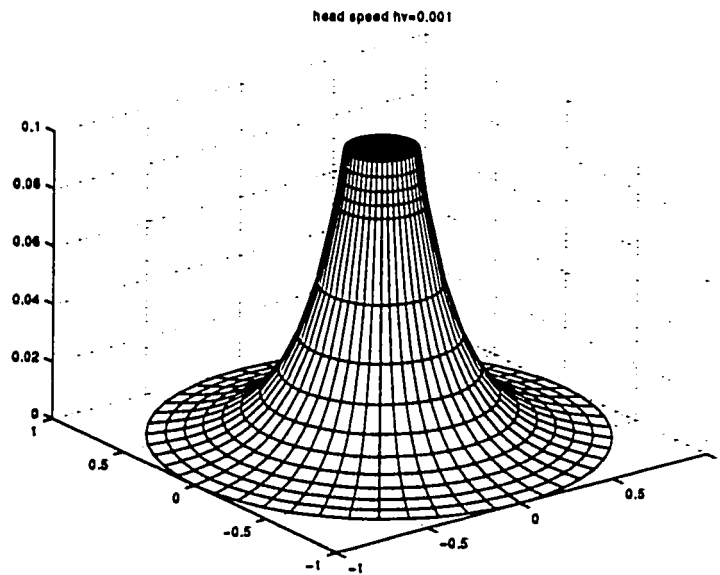


Figure 33: Deformed shape when $h\nu=0.001$

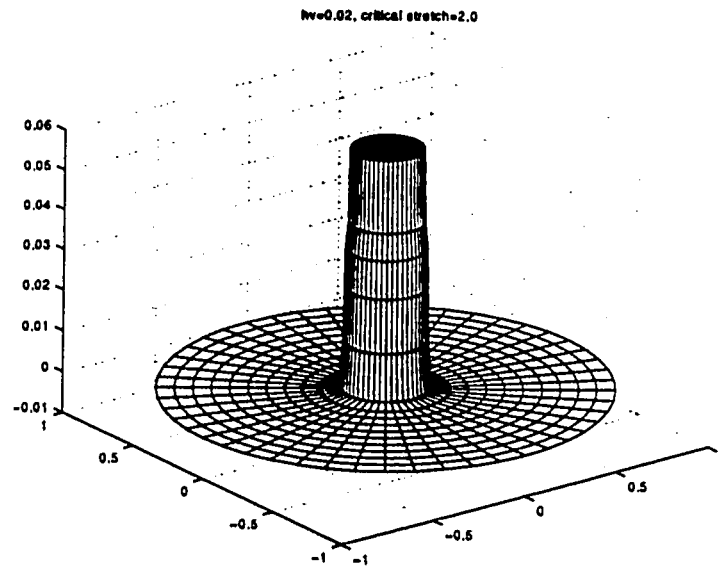


Figure 34: Deformed shape at initial punching stage

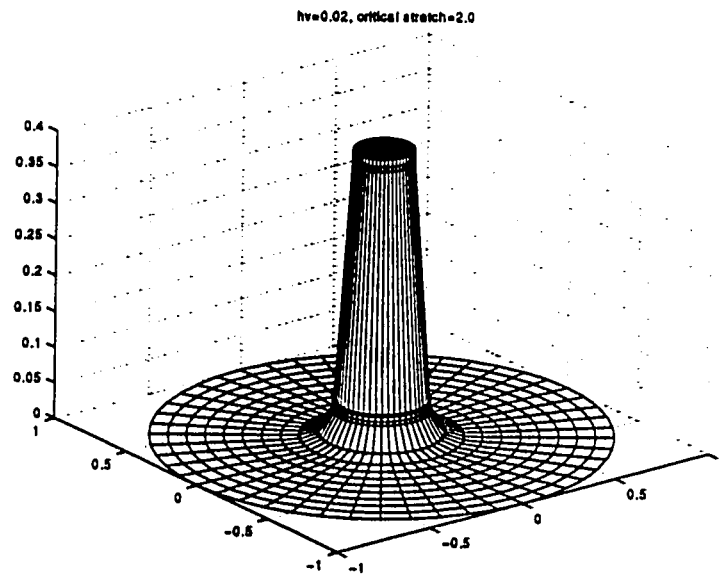


Figure 35: Deformed shape at broken stage

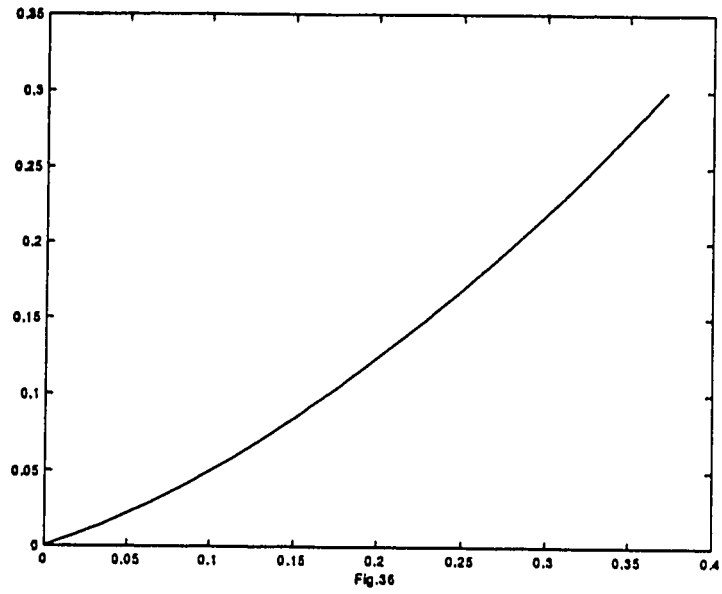


Figure 36: Static load-displacement relationship

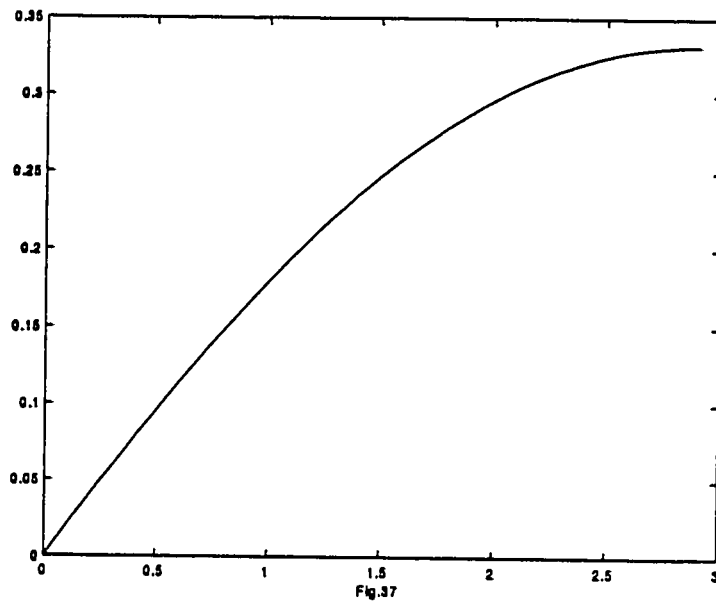


Figure 37: Motion of the mass

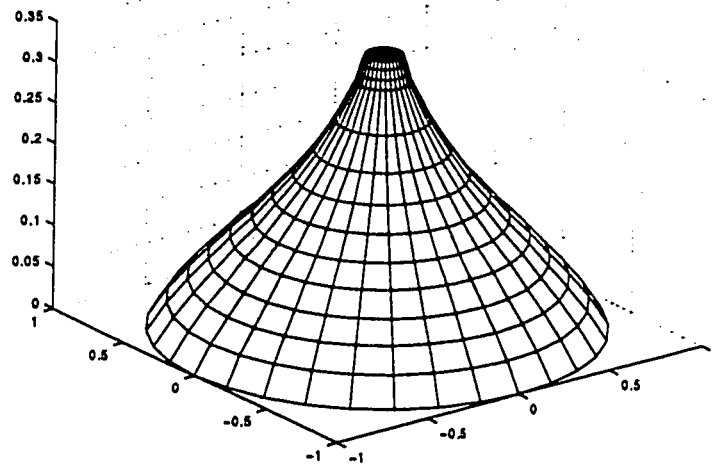


Figure 38: Deformed shape after being impacted

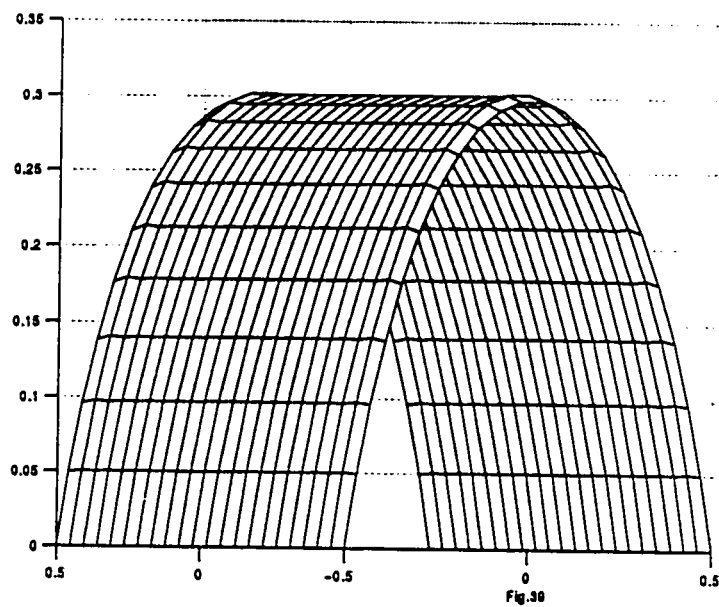


Figure 39: Deformed shape of unit square network

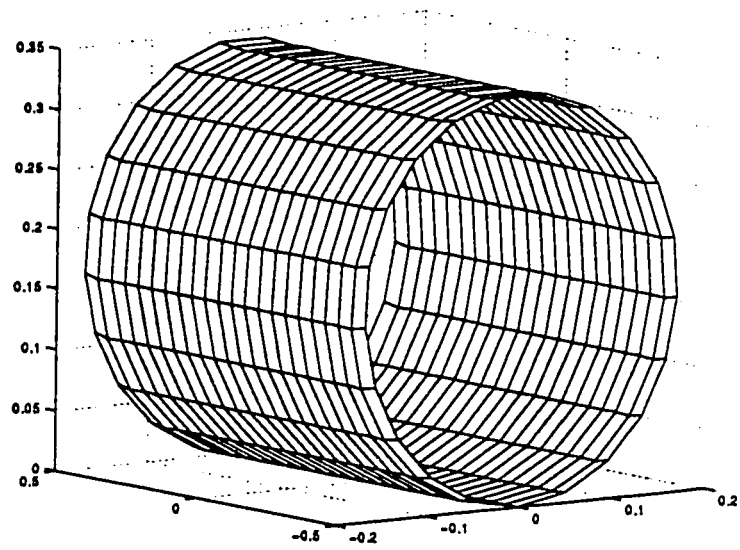


Figure 40: Deformed shape of unit square network

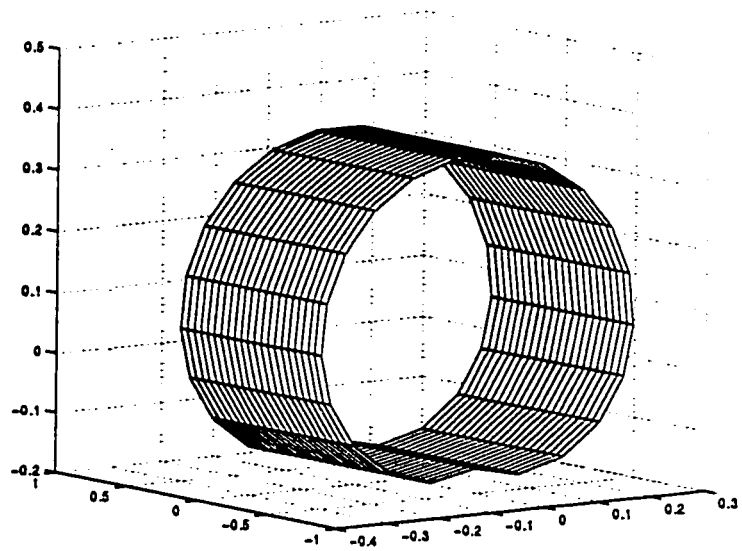


Figure 41: Deformed shape of circular cylinder network

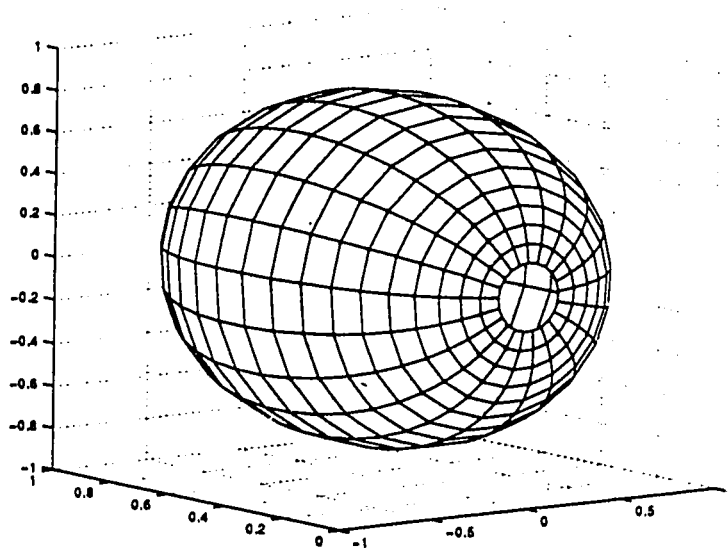


Figure 42: Deformed shape of circular cylinder network

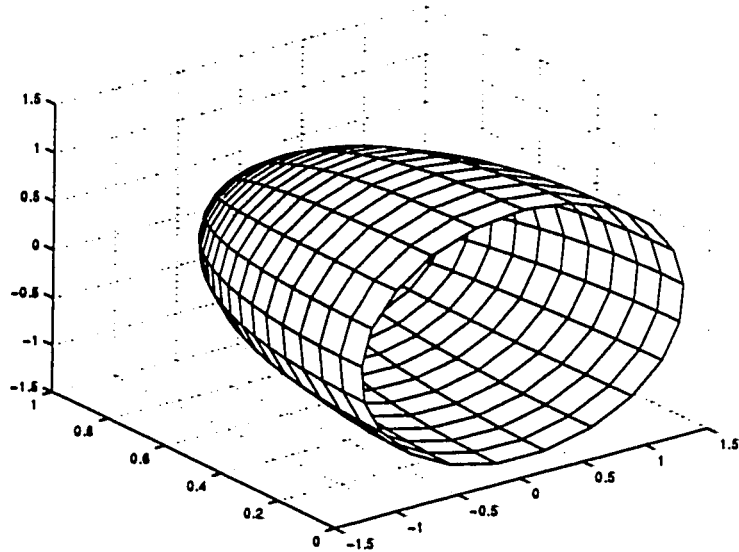


Figure 43: Deformed shape of circular cylinder network

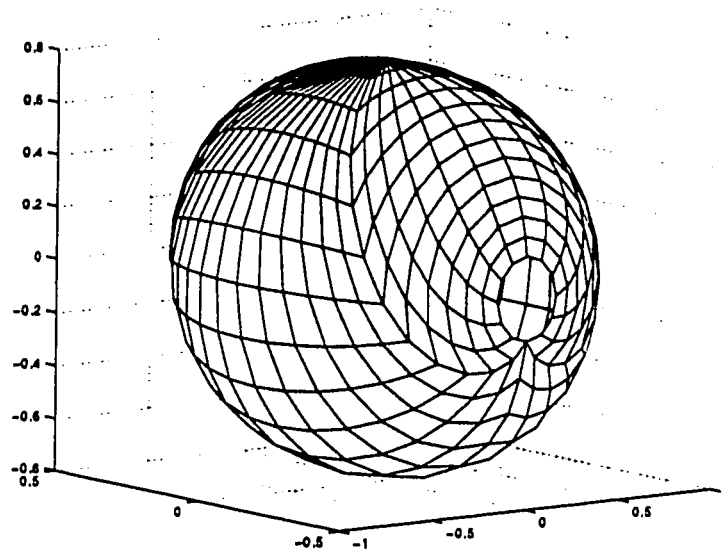


Figure 44: Deformed shape of circular cylinder network

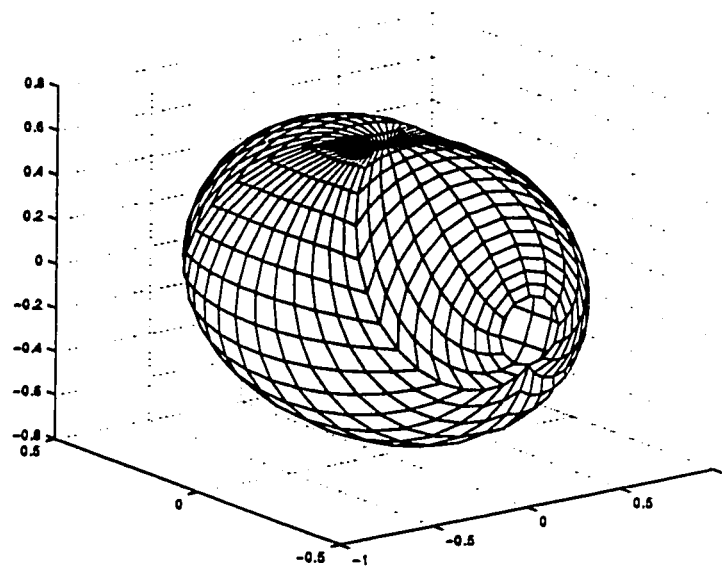


Figure 45: Deformed shape of circular cylinder network

Reference

- Adkins, J.E. 1956a Cylindrically symmetrical deformations of incompressible elastic materials reinforced with inextensible cords. *J. Rational Mech. Anal.* Vol.5, p.189.
- Adkins, J.E. 1956b Finite plane deformation of thin elastic sheets reinforced with inextensible cords. *Phil. Trans. Roy. Soc. London A*249, 125.
- Berger, H.M. 1955 A new approach to the analysis of large deflections of plates. *J. Appl. Mech.* 22, 465.
- Bushell D. 1977 A strategy for the solution of problems involving large deflections, plasticity and creep. *Int. J. Num. Meths. Engr.* Vol. 11, No. 4, pp. 683-728.
- Caridis, P.A.; Frieze, P.A. 1988 Flexural-torsional elasto-plastic buckling in flat stiffened plating using dynamic relaxation. *Thin-Walled Structures* 6 pp. 453-481.
- Cassel, A.C. 1970 Shells of revolution under arbitrary loading and the use of fictitious densities in Dynamic Relaxation. *Proc. Inst. Civ. Engrs.* 45 pp. 65-78.
- Föppl, A. 1907 *Vorlesungen über technische mechanik* Vol III, Teubner, Leipzig.
- Frieze P.A.; Hobbs R.E.; Dowling P.J. 1978 Application of dynamic relaxation to the large deflection elasto-plastic analysis of plates. *Computer & Structures* Vol. 8 pp. 301-310.
- Green, W.A.; Shi, J. 1990 Plane deformations of membranes formed with elastic cords. *Q.J. Mech. Appl. Math.* 43, 317-333.
- Gupta Aaron D.; Santiago Joseph M.; Wisniewski Henry L. 1980 An improved strain hardening characterization in the ADINA code using the mechanical sublayer concept. In: Conaway J.H. (eds.) *First CHAUTAUQUA on Finite Element Modeling*. PP. 335-351, Harwichport, Massachusetts, U.S.A.
- Han, P.S. and Olson, M.D. 1987 Interactive analysis of wind loaded pneumatic memberane structures. *Computers and Structures* 25 pp 699-712.
- Harding J.E.; Hobbs R.E.; Neal B.G. 1977 The elasto-plastic analysis of imperfect square plates under in-plane loading. *Proc. Instn Civ. Engrs* 63(part

2) pp. 137-158.

Haseganu, E.m.; Steigmann, D.J. 1994 Analysis of partly wrinkled membranes by the method of dynamic relaxation. *Computational Mechanics* 14 pp. 596-614.

Haseganu, E.M.; Steigmann, D.J. 1996 Equilibrium analysis of finitely deformed elastic networks. *Computational Mechanics* V17 n6 pp. 359-373.

Hearle, J.W.S., Grosberg, P., and Backer S. 1969 *Structural Mechanics of Fibers, Yarns, and Fabrics*, Wiley-Interscience, NY.

Hearle, J.W.S., J.J. Thaites, Jafirholi 1980 *Mechanics of Flexible Fiber Assemblies*. Sijthoff and Noordhoff.

Herrmann, W.; Bertholf, L.D. 1983 Explicit Lagrangian finite-difference method. In: Belytschko, T.; Hughes, T.J.R. (eds.) *Computational methods for transient analysis*, pp. 361-416. Elsevier, Amsterdam.

Jones, R. 1974 A simplified approach to the large deflection of membranes. *Int. J. Non-linear Mechanics* Vol. 9 pp 141-145.

Key, S.W.; Stone, C.M.; Krieg, R.D. 1981 Dynamic relaxation applied to the quasi-static, large deformation, inelastic response of axisymmetric solids. In: Wunderlich W. & Stein E. & Bathe K.J. (eds.) *Nonlinear Finite Element Analysis in Structural Mechanics*, pp. 585-620, Springer-Verlag Berlin Heidelberg New York.

Lim, G.J.; Turvey, G.J. 1984 Full-range response of uniformly loaded clamped circular steel plates - comparison between theory and experiment. *Proc. Inst. Civil Enhrs.* 77 p. 139.

Oden, J.T. 1972 *Finite elements of nonlinear continua* McGraw-Hill, New York.

Paul Seide 1977 Large deflections of rectangular membranes under uniform pressure. *Int. J. Non-linear Mechanics*, Vol. 12, PP. 397-406.

Petr Rericha 1986 Optimum load time history for non-linear analysis using dynamic relaxation. *Int. J. Num. Meths. Engr.* Vol. 23 PP. 2313-2324.

Rivlin, R.S. 1955 Plane strain of a net formed by inextensible cords. *J. Ration. Mech. Anal.* 4, 951.

Rivlin, R.S. 1959 The deformation of a membrane formed by inextensible

cords. Arch. Ration. Mech. Anal. 2, 447.

Rushton K.R.; Hook, P.M. 1974 Large Deflection of Plates and Beams Obeying Non-linear Stress-Strain Laws. J. of Strn. Ana. Vol. 9 No. 3 pp. 178-184.

Steigmann, D.J. & Pipkin, A.C. 1991 Equilibrium of elastic nets. Phil. Trans. R.Soc. A 335, PP. 419-54.

Steigmann, D.J. 1992 Equilibrium of prestressed networks. IMA Journal of Applied Mathematics, Vol. 48 pp. 195-215.

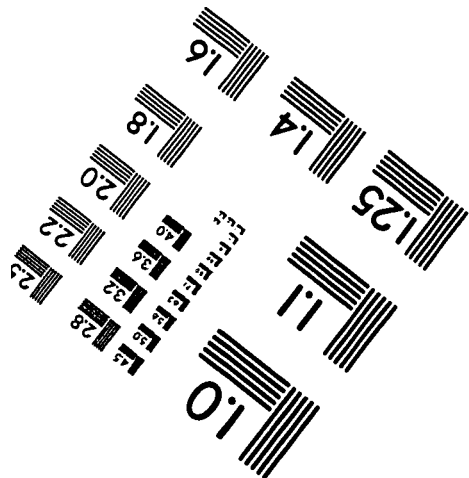
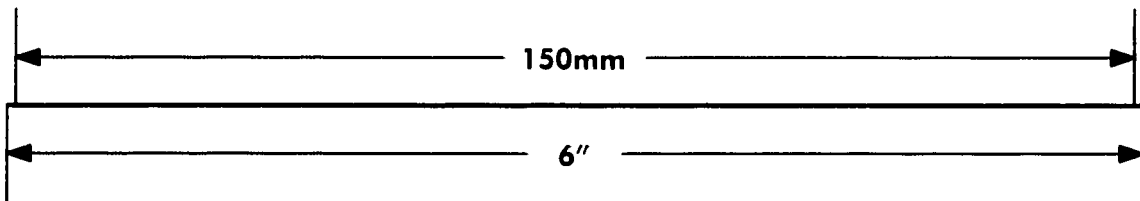
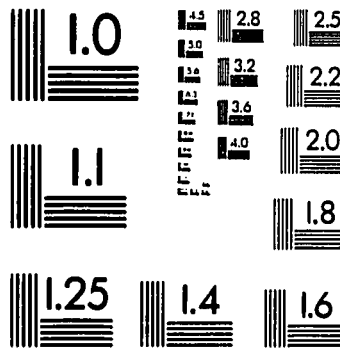
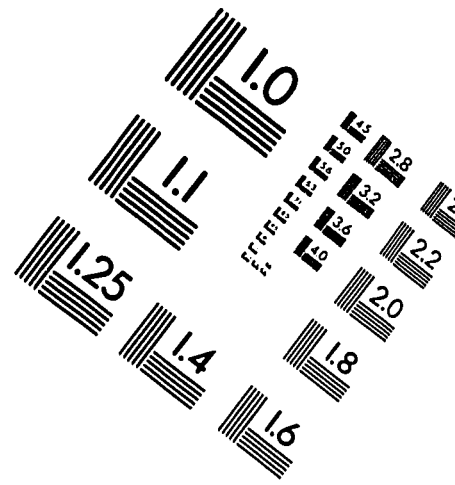
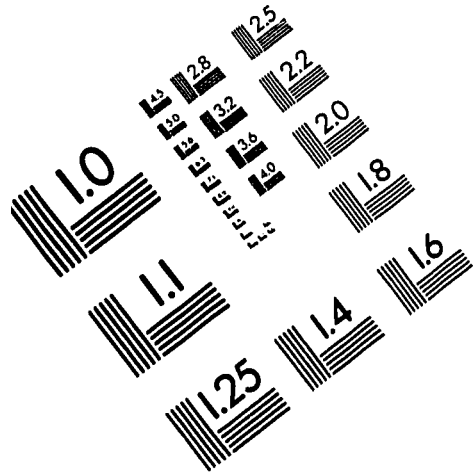
Tchebychev, P.L. 1878 Sur la coupe des vetements. Assoc. Franc. pour. l'avancement des sci., Congres des Paris, 154.

Turvey, G.J. 1979 Axisymmetric elasto-plastic flexure of circular plates in the large deflection regime. Proc. Inst. Civil Eng. 67 pp. 81-92.

Underwood, P. 1983 Dynamic relaxation. In: Belytschko, T; Hughes, T.J.R.(eds.) Computational methods for transient analysis, pp. 245-265. Elsevier, Amsterdam.

Zvi Rigbi and Yael Hiram 1981 An approximation method for the study of large deformations of membranes. Int. J. Mech. Sci. Vol. 23 pp 1-10.

IMAGE EVALUATION TEST TARGET (QA-3)



APPLIED IMAGE, Inc
1653 East Main Street
Rochester, NY 14609 USA
Phone: 716/482-0300
Fax: 716/288-5989

© 1993, Applied Image, Inc., All Rights Reserved

